

Todor Emilov Vlakhov

Nanostructured soft matter, studied by optical methods, complex impedance and dielectric spectroscopy

SUMMARY

of a dissertation for an educational and scientific degree "PhD"

professional field: 4.1 Physical Sciences
scientific specialty "Condensed Matter Physics"

PhD program Condensed Matter Physics

Scientific supervisors: Prof. D.Sc. Yordan Marinov
Prof. Georgi Hadjichristov

Reviewers

Prof. D. Sc. Vera Marinova

Prof. D. Sc. Minko Petrov

The dissertation consists of 125 pages, 51 figures and 139 cited literature sources and it contains of an introduction and 5 parts. The first part of the dissertation is a review of soft matter materials such as liquid crystals, polymer electrolytes and LB films. The second part includes the aim and tasks of the dissertation. The next part presents the materials used and research methods employed. The fourth part discusses the experimental results obtained, and the fifth part presents the conclusions and contributions from the study of nanostructured soft matter.

The thesis was discussed and directed for defense by scientific seminar of the Department of Soft Matter Physics, Institute of Solid State Physics - BAS, held on 07.10.2025.

http://www.issp.bas.bg

ISSP-BAS-2025-PhD030

The defense of the dissertation will take place on 28.01.2026 at 14:00 time in hall 300 of the ISSP - BAS, 72 "Tsarigradsko shose" blvd.

scientific jury:

- 1. Prof. Antonia Stoyanova IEES- BAS
- 2. Prof. D.Sc. Vera Marinova IOMT- BAS
- 3. Prof. Ivalina Avramova IGIC- BAS
- 4. Assoc. Prof. Angelina Stoyanova-Ivanova ISSP- BAS
- 5. Prof. D. Sc. Minko Petrov ISSP- BAS

Contents

Used abbreviation	5
Introduction	6
Relevance of topic	7
Aim and tasks	8
3.1. Materials used and research methods	9
3.1.1.Materials and methods for preparing polymer	
nanocomposites PEO/PVP/NaIO ₄ /TiO ₂ and PEO/PVP/NaIO ₄ /GO	9
3.1.2. Materials and methods for obtaining nanostructured liquid	
crystals by adding nanoparticles	11
3.1.2.1. Materials and methods for preparing graphene/liquid	
crystal nanocomposite E7	11
3.1.2.2. Materials and methods for preparing polymer liquid crystal co	mposites
PEO/E8 and PEO/E8/NaIO4	12
3.1.3. Materials and methods for preparing nano-thin Langmuir-Blodget	t
(LB) films	12
3.2. Methods of studying/ research the obtained nanocomposites	14
3.2.1. XRD	14
3.2.2. SEM	14
3.2.3. Polarization microscope	14
3.2.4. EIS	15
3.2.5. Micropipette - drop technique	18
3.2.6. Method for detection of vapours of volatile organic compounds	19
Results and Discussion	19
4.1. Investigation of polymer electrolytes	19
4.1.1. Polymer electrolyte PEO/PVP/NaIO4/TiO2	19
4.1.2. Polymer electrolyte PEO/PVP/NaIO4/GO	23

4.2. Investigation of composites and nanocomposites based on liquid crystals	28
4.2.1. Investigation of a nanocomposite of nematic liquid crystal E7 and graphene	28
4.2.2. Investigation of polymer-liquid crystal composites (PEO/E8)	32
4.3. Investigation of LB films	4(
4.3.1. Detection of heavy metal ions by a newly designed biosensor	4(
4.3.2. Phospholipid Langmuir-Blodgett films and impedance spectroscopy	
for the detection of acetone and methanol vapours	44
Conclusions and Contributions	48
Conclusions	48
Contributions	50
List of scientific publications	50
List of scientific presentations	53
References used in dissertation summary	56

Used abbreviation

PEO - Poly(ethylene oxide)

PVP - Polyvinyl pyrrolidone

LC - Liquid Crystals

E7 - Nematic liquid crystals

E8 - Nematic liquid crystals

LB - Langmuir-Blodgett films

DPPE - Phospholipid dipalmitoyl-phosphatidyl-ethanolamine

NBD - NitroBenzoxaDiazole

SAWR - Surface Acoustic Wave Resonator

IDEs - Interdigital electrodes

XRD - X-ray diffraction analysis

SEM - Scanning electron microscopy

EIS - Electrical impedance spectroscopy

VOC - Volatile Organic Compounds

NCSPEs - Nanocomposite solid polymer electrolyte

SPE- Solid polymer electrolyte

NPs - Nanoparticles

PLCCs- Polymer/Liquid Crystal Composites

Introduction

In the times of the present epoch of fast advancing science and technology, creation and investigation of new materials with specific properties become of key importance for the breakthrough / advancements in different fields as physics, biophysics, electronics, pharmacy, medicine and sensor technology. Progress in the important technology areas often is due to creation and employing of new materials and structures that are superior to used ones. Development and tailoring of materials at atomic and molecular level, aiming creation of new properties and functionalityes, sounds as pretty modern conception.

Technologies of new millenium require and need not only development of innovative materials, but also signitific changes in the investigation/scientific approach aiming miniatuarisation of components and devices, its adaptivity and compatibility to new approaches and advances in the fields of optic, microelectronics, data translation and analysation, broadcasting, Artificial Intelegence employment, as well as better energy effectivity and self sustainability. "Soft matter" term coined during twenty century [1] includes materals like polymers and liquid crystals. Liquid crystal (mesomorphic matter) is the state between solid crystal and isotropic liquid [2-4]. LC are very promissing for applications in organic electronic devices. Introducing different types of nanoparticles into material, like graphene, etc, results in multifunctional materials with improved properties, like better electrical and dielectrical characteristics. The solid and flexible composites, consisted by polymers and LC, are another type multifunctional materials with great potential. They possess appropriate /suitable mechanical, electrical, dielectric, and thermic properties.

The synthetic polymer Poly(ethylene oxide) (PEO) is often used as a polymer matrix in polymer–salt composites' electrolytes. PEO has semi-crystalline structure which makes it suitable as a host for alkali metal ions (Na⁺-ions) and supports ionic conductivity. There are known many investigations on mixture of PEO and PVP as well as suitable salt dopants, which showed deteriorated crystallinity of polymer matrix and increase of ionic conductivity. ISSP - BAS possess many advancements and traditions in area of investigations on soft matter and LC which becomed good basement for further development of new multifuntional materials.

New nanostructured materials of different types as polymer nanocomposites PEO/PVP/NaIO₄/TiO₂ and PEO/PVP/NaIO₄/GO, graphene/LC E7 nanocomposite, polymer-liquid crystal composites PEO/E8, PEO/E8/NaIO₄, Phospholipid Langmuir-Blodgett films are prepared and investigated in the frame of present dissertation work. Micropipette - drop technique was developed. Such an approach, allowing the necessary surface contact and precise localization, was used to bring a millimeter-size patch of lipid monolayer deposited on solid substrate into contact with a drop-formed electrolyte (in our case, aqueous solution of KCl at concentration 150mM). The impact of the TiO₂

or GO NPs on AC conductivity and electrical conductivity of the complex NCSPE system PEO/PVP/NaIO₄ was established.

The optical, electrical and dielectric properties of these nanocomposites have been studyed using modern methods, and the parameters of ionic conductivity and dielectric relaxation have been evaluated in order to assess their suitability for applications in various fields such as telecommunications, sensors, organic electronics, in energy storage devices (sodium-ion polymer batteries), etc. The results obtained by the dissertation work are a part of global scientific investigation process in apropriate fields, which is evidenced by the citations of our publications.

The presented dissertation work is divided into 5 parts. The first part of the dissertation is a review of soft matter materials such as liquid crystals, polymer electrolytes and LB films. The second part includes the aim and tasks of the dissertation. The next part presents the materials used and research methods employed. The fourth part discusses the experimental results obtained, and the fifth part presents the conclusions and contributions from the study of nanostructured soft matter.

Relevance of topic

The elaboration and optimisation of innovative materials are of decisive importance for development of today technologies and have to play key role in global scientific and technological advancement. Recently research approaches have directed to solve appeared basic technology problems as optimisation and miniaturisation of device components, better energy efficiency and device functionality independence. ISSP BAS possess many advancements and traditions in area of investigations on soft matter and LC, which is a prerequisite for search of innovative materials based on them and development of new multifuntional materials.

Generally, the incorporation of proper nanoparticles (NPs) into suitable polymer matrix may substantially improve the electrical performance of the resultant polymer-based nanocomposite without sacrificing the mechanical strength of the material.

Aim and tasks

The aim of the dissertation is to obtain new nanostructured materials from soft matter and study their optical, electrical and dielectric properties.

Tasks:

- 1. Preparation and study of polymer electrolytes. Characterization of their functionality
- 2. Preparation and study of nanostructured liquid crystals with added nanoparticles
- 3. Study of biosensor properties of nano-thin Langmuir-Blodgett (LB) films

3.1. Materials used and research methods

3.1.1. Materials and methods for preparing polymer nanocomposites PEO/PVP/NaIO₄/TiO₂ and PEO/PVP/NaIO₄/GO

In this dissertation we used the polymers Polyethylene Oxide (PEO) (Figure 1) [5] and Polyvinylpyrrolidone (PVP) (Figure 2) [5] to prepare the nanocomposites PEO/PVP/NaIO₄/TiO₂ and PEO/PVP/NaIO₄/GO.

Polyethylene oxide (PEO) is a long-chain linear polymer composed of repeating units of ethylene oxide. The molecular weight of PEO can vary, which affects its physical and chemical properties. It often has a molecular weight in the range of 100,000 to several million Daltons. Polyethylene oxide (PEO) is a versatile polymer that finds wide application in various industries due to its diverse properties: highly water. high viscosity and exhibits thermoplastic behavior. soluble Polyvinylpyrrolidone (PVP) is a water-soluble polymer compound made from the monomer N-vinylpyrrolidone. PVP is soluble in water and other polar solvents. When dry it is a light flaky hygroscopic powder, readily absorbing up to 40% of its weight in atmospheric water. In solution, it has excellent wetting properties and readily forms films. This makes it good as a coating or an additive to coatings. PVP is also used in many technical applications: as a special additive for batteries, ceramics, fiberglass, inks, and inkjet paper, and others.

Figure 1.Molecular structure of poly(ethylene oxide) (PEO)

Figure 2.Molecular structure of polyvinyl pyrrolidone (PVP)

PEO and PVP, were procured from Aldrich and employed without any further purification to prepare the polymer blend electrolytes (figure 3a and 3b). The salt

Sodium metaperiodate (NaIO₄), Titanium dioxide (TiO₂ nanopowder) and GO nanosheets, were used as additives. All substances were dissolved in methanol with high purity from Aldrich. First, PEO and PVP polymers were individually dissolved in methanol, then appropriate amounts of PEO and PVP solutions (w/w ratio 70%: 30% in present experiments) were mixed, followed by mechanical stirring at room temperature for 15 hours to obtain uniform mixture. In the meanwhile, 10 wt% of NaIO₄ salt was separately dissolved in methanol and this solution was added to the prepared viscous PEO/PVP polymer solution in order to be produced PEO/PVP/NaIO₄ polymer complex. Separately, the powder of nano-sized TiO₂ or GO was homogeneously dispersed in methanol. Their solutions was sonicated for 30 minutes and then added to PEO/PVP/NaIO₄ solution to prepare nanocomposite PEO/PVP/NaIO₄/TiO₂ and PEO/PVP/NaIO₄/GO. Nanoparticles TiO₂ and GO were included in the polymer mixture in concentrations (1-5 wt. % TiO₂ and 0,2; 0,4; 0,6 wt. % GO). Chemicallystable free-standing thin films of the synthesized nanocomposites are formed by using solution casting of nanocomposite blend solution. The as-prepared viscous nanocomposite blend solutions were poured into polypropylene dishes and the solvent (methanol) was allowed to evaporate slowly at room temperature to obtain free-standing polymer electrolyte films of thickness of 100- 150 μm.

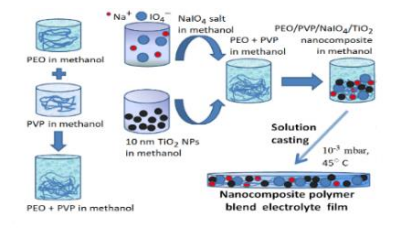


Figure 3a) A scheme showing the preparation of PEO/PVP/NaIO₄/TiO₂ solid-state nanocomposite polymer electrolytes.

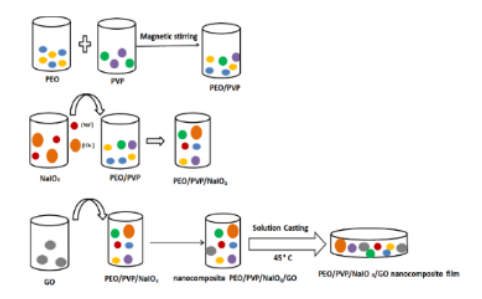


Figure 3b) A scheme showing the preparation of PEO/PVP/NaIO4/GO solid-state nanocomposite polymer electrolytes.

3.1.2. Materials and methods for obtaining nanostructured liquid crystals by adding nanoparticles

3.1.2.1. Materials and methods for preparing graphene/liquid crystal nanocomposite E7

Nematic liquid crystal E7 and graphene nanoparticles with a low concentration (10⁻³ wt %) (Figure 4) were used to prepare the graphene/liquid crystal E7 nanocomposite. The LC mixture E7, composed of 4-cyano-4'-n-pentyl-biphenyl (5CB), 4-cyano-4'-n-heptyl-biphenyl (7CB), 4-cyano-4'-n-octyloxy-biphenyl (8OCB), and 4-cyano-4"-n-pentyl-p-terphenyl (5CT), has been widely used in LC devices due to its large birefringence (Figure 5) [6].

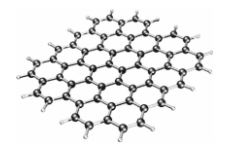


Figure 4. Crystal structure of graphene nanoparticles.

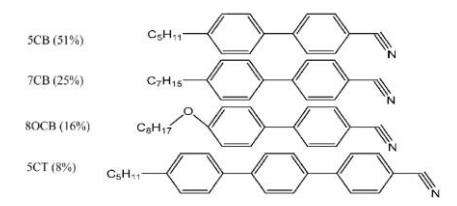


Figure 5. Composition and chemical structure of the individual components of liquid crystal E7.

The E7 mixture has not been modified in any way before the nanocomposite preparation. To prepare graphene-E7 nanocomposite, graphene was added at the concentration of 10⁻³ wt.% to the LC E7. This mixture was centrifuged for 30 min at 4000 rpm to make the constituents uniformly mixed, then heated above 60 °C to reach isotropic phase of the LC. The heated graphene-E7 dispersion was capillary filled into standard LC sandwich cells. Finally, the nematic phase of the E7 LC containing graphene was recovered. The LC cells were assembled with two 1 mm-thick 15 mm ′ 25 mm glass plates having their inner surfaces coated with conductive indium-tin oxide (ITO) and a polyimide alignment layer for planar orientation. The gap of the cells was d = 7 μm. Besides the graphene-doped E7 layers with planar alignment, layers with the

same dimensions were prepared by the same manner, but filled with E7 only (for reference measurements).

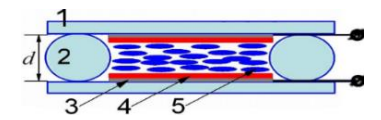


Figure 6. Schematic of planarly-aligned LC cell: 1 – the plane glass/ITO substrate, 2 – spacer, 3 – plane electrode (of ITO), 4 – alignment layer, 5 – elongated rod-like LC molecule (E7)

3.1.2.2. Materials and methods for preparing polymer liquid crystal composites PEO/E8 and PEO/E8/NaIO4

The materials used to produce these composites include the polymer Polyethylene Oxide (PEO) and the liquid crystal E8 in a nematic phase. The composition of this nematic LC is shown in Figure 7 [7]. Polymer/LC composites were produced from PEO and LC E8 via their mixing at a ratio PEO:E8 = 70:30 by weight (wt.%). This ratio was found to be optimal for both the ion conductivity and dielectric properties of these composites. To produce PEO/E8/NaIO₄ ion-polymer complexes, the salt sodium metaperiodate (NaIO₄) was added at a concentration of 10 wt.% to the PEO/E8 composite. The compositional ratio was PEO:E8:NaIO₄ = 63:27:10 wt.%. Such content of NaIO₄ ensured a fairly good ion conductivity and suitable dielectric permittivity of the PEO/E8/NaIO₄ electrolyte films without changing the other properties, quality and long-term stability [8]. Free-standing, flexible thin films with a thickness of 150 μ m. of both PEO/E8 and PEO/PVP/NaIO₄ were prepared by the conventional solution cast technique

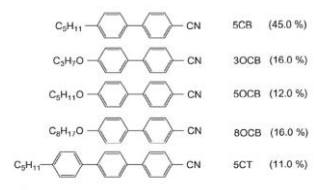


Figure 7. Composition and chemical structure of the individual components of liquid crystal E8

3.1.3. Materials and methods for preparing nano-thin Langmuir-Blodgett (LB) films

The Langmuir-Blodgett (LB) films studied in this thesis were prepared from the phospholipid Dipalmitoylphosphatidylethanolamine (DPPE) labeled with

nitrobenzoxadiazole (NBD) (Figure 8) [9]. DPPE-NBD was purchased from Avanti Polar Lipids (USA) in chloroform solution at a concentration of 1 mg/ml and is of claimed purity of 99.5%.

The thin films were deposited on an electrically conductive glass substrate and onto the active area of Surface Acoustic Wave Resonator (SAWR). At the top surface of the SAWR device was patterned metal (gold) interdigitated microelectrode structure (IDEs) (Figure 9). The thickness of the DPPE LB films deposited on the SAWR was about 3 nm.

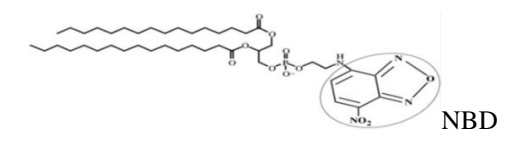


Figure 8. Molecular structure of phospholipid DPPE- NBD

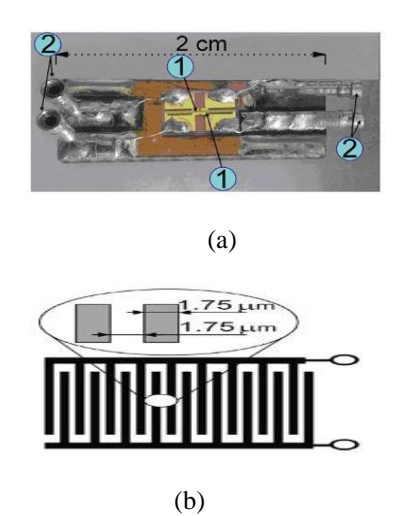


Figure 9. (a) Quartz SAW device with two sets of interdigital gold electrodes (1) in series on the surface; (2) external terminals.

b) Schematic (top view) of interdigital electrodes consisting of two interlocking combshaped arrays.

3.2. Methods of studying/ research on the obtained nanocomposites

To achieve the aim of the dissertation we used the following structure characterization methods: X-ray diffraction analysis (XRD), SEM, Polarization microscope, EIS, Micropipette - drop technique, method for detecting vapours of volatile organic compounds.

3.2.1. XRD

The structural properties of nanocomposite PEO/PVP/NaIO₄/GO were analysed by recording X-ray diffraction patterns in the 2θ range of $10^{\circ}-80^{\circ}$ with a constant step 0.020, counting time 35s/step on a Bruker D8 Advance diffractometer with Cu K α radiation and LynxEye detector.

3.2.2. SEM

The scanning electron microscope is a type of electron microscope used to study and magnify objects. The scanning electron microscope provides information about:

- Topography of the sample the objects on its surface, limited to a depth of a few nm
- Morphology of the sample size, shape and arrangement of particles in the sample, formation of aggregates, etc.
- Information about the chemical composition the elemental composition of the sample.

These capabilities make the method widely used in various fields such as physics, chemistry, ecology, medicine, materials science, etc. SEM studies of polymer electrolytes PEO/PVP/NaIO4/GO in this dissertation were performed with a "SEM Philips 515 digitalized".

3.2.3. Polarization microscope

A polarizing microscope is a type of optical microscope. Its device is characterized by a polarizer located below the condenser (converts the light passing through it into linearly polarized), and an analyzer located above the objective (it determines the plane of polarization of the light emerging from the object). In this dissertation, optical studies of the PEO/E8 sample were performed with a NU-2 universal polarizing optical microscope (Carl Zeiss Jena) under conditions of crossed polarizer and analyzer and without polarizers.

3.2.4. EIS

The methods based on the excitation of an object by a sinusoidal signal were first employed as a way of measuring the rate constant of fast electron transfer reactions at short times. The principle of Electrochemical Impedance Spectroscopy (EIS) is to perturb the obect with an alternative signal, and to observe how the systems follows the perturbation at the steady state (the amplitude of perturbation should be small in order to assume the linear behaviour of the system). EIS is frequently employed for investigation on corrosion, battery, fuel cell development, sensors and biosensors, fundamental electrochemistry, semiconductors, nano- and biotechnologies, etc. [10, 11]. EIS uses basic equation Z = Z' - iZ'', where $i = \sqrt{-1}$, Z' - real part of resistance (active part), Z'' - imaginery part of the resistance (reactive part). This equation can provide valuable information on reaction parameters, corrosion rates, electrode surfaces porosity, coating, mass transport, and interfacial capacitance measurements.

EIS could be represented by two basic ways 10]. Nyquist plot presents Z'' vs. Z' dependence (see Figure 10) [10] and gives also information on the bulk resistance value - (R_{Ω}), charge transfer resistance value - (Rct), as well as to indicate appearance of diffusion process. The second method to present EIS data is so called Bode plot (see Figure 11) [10] which represents frequency dependecies of both parts of the impedance, namely (Z'' vs. f) and (Z' vs. f) dependences. It is well establish that the combination of both plots gives enough information on the entire behaviour of the investigated system. When working in the frequency domain, over a wide range of frequencies, EIS simplifies a complex electrochemical system by deconvoluting it in individual processes with different time constants, which then can be easily analyzed. (Very) slow processes can be probed in (very) low frequencies, while (very) fast processes can be probed in (very) high frequencies.

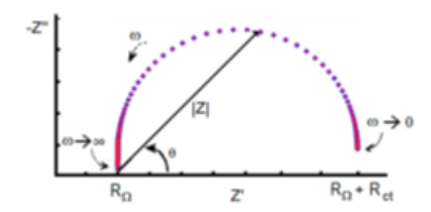


Figure 10. Nyquist plot

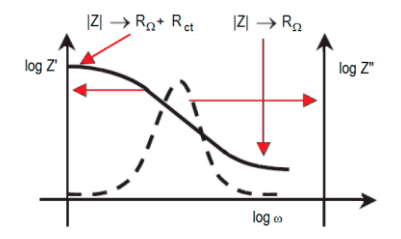


Figure 11. Bode plot

The commersially available equipment (Working station SP-200, Bio-Logic Science Instruments) had ensured EIS measurements in potentiostatic as well as galvanostatic regime (see Photo N $\!$ 1). Te device is employed for scientific experiments in the frequency range 0.1 Hz - 3 MHz. Additionally, equipment is provided by Ultra-Low-Current Sonde (see Photo N $\!$ 2) with available currents values in the range 1pA - 500mA. This equipment was used for characterizing of all prepared by this dissertation work samples of different nanostructured materials.



Photo 1. Working station SP-200, Bio-Logic Science Instruments, where 1-commecting cable (USB cable), 2 – Potentiostat / galvanostat connecting cable



Photo 2. Ultra-Low-Current Sonde in the range 1pA - 500mA.

The term impedance was coined by Oliver Heaviside in July 1886. The impedance represents the entire value of resistance comprised by active, inductive and capacitive parts of electrical resistance.



Figure 12. EIS measurements

EIS measurements were performed by Input signal current (I) and Output signal voltage (U), see Figure 12 [12].

Two-electrode connection (see Figure 13) [13] is usually employed in investigation of two-poles samples like thin films, semiconductors, LC cells, etc.

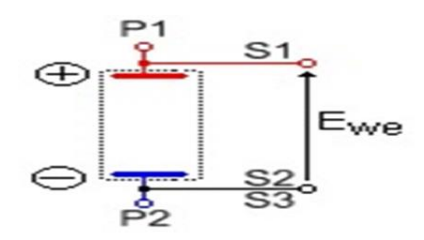


Figure 13. Two-electrode connection.

The Potentiostatic EIS experiment performs impedance measurements into potentiostatic mode by applying a sinus around a potential E that can be set to a fixed value or relatively to the cell equilibrium potential (see Figure 14) [13].



Figure 14. Potentiostatic electrical impedance spectroscopy.

Working station SP-200 was used to characterize all samples obtained in the frame of present dissertation (composites and nanocomposites) in the frequency range 0.1 Hz - 1 MHz.

3.2.5. Micropipette - drop technique

The electrical measurements were performed by applying a micropipette-drop technique (Figure 15) that utilizes a modified electrode interface of a well-controlled drop of electrolyte. Such an approach allowing the necessary surface contact and precise localization was used to bring a millimeter-size patch of lipid monolayer deposited on solid substrate into contact with a drop-formed electrolyte (in our case, aqueous solution of KCl at concentration 150mM). By means of syringe attached to pipette holder, liquid electrolyte drops were formed on the tips of the glass micropipette (outer/inner diameter equal to 1.5mm/0.86mm). By the electrical measurements, the millimeter-sized drop of liquid electrolyte (a drop formed by micropipette) was used as a counter electrode. An Ag/AgCl wire was inserted into the pipette before its filling with the electrolyte. The ITO layer serves as a working electrode. By use of drop interface, one can avoid the imperfection of the layer structure due to the edge effects. Moreover, a desirable area on the sample surface can be selected.

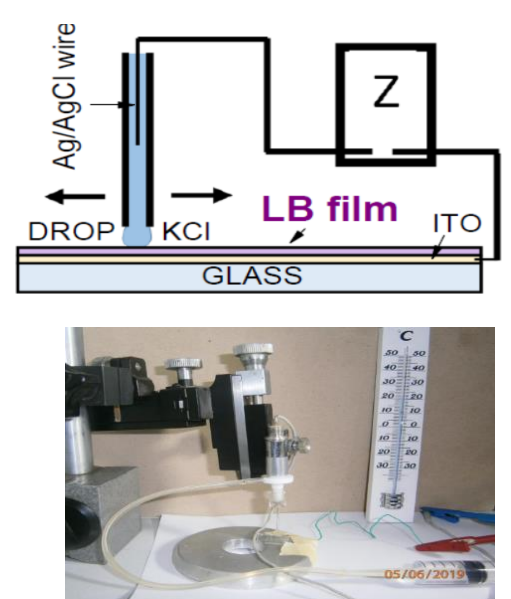


Figure 15. Schematic of the experimental set-up and micropipette drop technique.

3.2.6. Method for detection of vapours of volatile organic compounds

The experimental set-up used in this dissertation is illustrated in Figure 16. The examined gas detector element, composed of DPPE LB film deposited on interdigitated microelectrodes, was placed inside a glass exicator and connected to an electrical impedance-meter (outside the exicator). Liquid VOC in a Petri dish was evaporated at constant temperature in the exicator. The vapour concentration was determined by measurement of the weight loss of the liquid VOC in the dish by means of sensitive electronic balance. The experiments were conducted after temperature stabilization of the exicator. During the measurements, the temperature was kept fixed at 26 ± 0.1 °C, outside as well as inside the exicator.

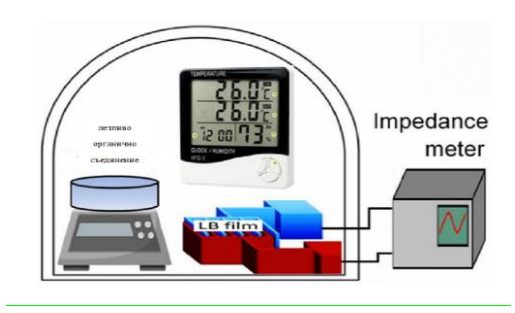


Figure 16. Experimental setup for detection of volatile organic compounds.

Results and Discussion

4.1. Investigation of polymer electrolytes

4.1.1. Polymer electrolyte PEO/PVP/NaIO₄/TiO₂

Raw experimental data were obtained by complex electrical impedance spectroscopy. By this experimental technique both real (Z') and imaginary (Z'') parts of the complex electrical impedance $Z^* = Z' + iZ''$ are simultaneously measured as a function of the frequency f of the AC electric field applied on the sample. The intensity of the oscillating electric field is low, but enough to probe the dipolar character of the electrolyte materials under study.

Figure 17 presents the recorded frequency spectra Z' (f) and Z' (f) of the impedance of PEO/PVP/NaIO₄/TiO₂ NCSPEs. It is seen that the frequency behaviours relevant to the concentrations of TiO₂ of 2–5 wt% considerably differ from those at TiO₂ concentrations 0 and 1 wt%. It is useful to remember that Z' is linked to the Ohmic

resistance while Z" takes into account the non-Ohm resistances. The maximum of Z" parts corresponds to the value of the frequency fmaxZ" parts at which the main dielectric active relaxation of the system occurs under the action of an AC electric field. In the low-frequency range (f < fmaxZ") it is noted that (-Z") < Z' (Fig. 17 b). This peak in the imaginary (Z") part originates from the orientation of the dipoles (the interplay between the resistance and the capacity of the samples). In the case of a pure dielectric, Z" has only one (dielectric) relaxation peak, therefore only one relaxation time constant = $(2\pi f)^{-1}$ (called Debye relaxation). The Z"(f) spectra (Figure 17 b) suggest that as the percentage of TiO₂ NPs increases, the orientation of the dipoles becomes more complex. The maximum of Z" is shifted towards the higher frequencies, from fmax 10 kHz up to 0.5 MHz, with a jump between the TiO₂ NPs values of 1 wt% and 2 wt%. At higher concentrations, up to 5 wt%, the maximum of Z" remains almost constant and this points towards saturation value. The observed shift of the Z" peak means a decrease in the dielectric relaxation time.

The observed saturation of the dielectric relaxation means that the presence of TiO_2 NPs at concentration above 3 wt% (in our case, 4–5 wt%) in the polymer matrix is not favourable for the enhancement of polymer chain segmental motion. The evidence of a minimum in the imaginary (Z'') part (Fig. 17 b), at the frequency f_{min} , indicates the accumulation of charges in the electrode-electrolyte interfacial region (a double layer which has an extremely high resistance value at low frequencies). The presence of a double layer (electrode polarization) affects the relaxation and the dispersion of relaxation times. The Z'' spectra (Fig. 17 b) imply that there is no ideal Debye relaxation.

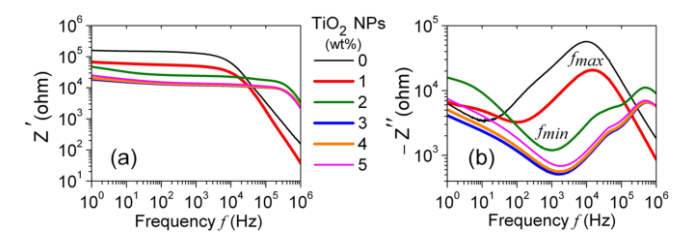


Figure 17. Frequency spectra of: (a) real part (Z'); (b) imaginary part (Z") of complex electrical impedance for the studied PEO/PVP/NaIO₄/TiO₂ NCSPEs measured under identical experimental conditions and various concentration (wt%) of TiO₂ NPs

The effect of TiO_2 NPs on the electrical properties of PEO/PVP/NaIO₄/TiO₂ samples can be seen in the Nyquist plots (real (Z') versus imaginary (Z") complex diagrams) (Fig.18). The impedentiometric responses of the studied NCSPEs consist of semicircle arcs on the high-frequency side, followed by a steep line (forming an inclined spike) at the low-frequency side. This shape confirms the typical ionic behaviour of the studied NCSPE. The semicircle corresponds to the bulk effect of the polymer electrolyte and this is the characteristic of ionic conduction. Such a shape is relevant to the

equivalent circuit of capacitance and resistance connected in parallel. In the lower-frequency region, the gradual increase of Z" values as the frequency decreases indicates a build-up of electric double-layer capacitance at the electrode/electrolyte interface. The value of the bulk resistance (Rb) of the material was determined from the (extrapolated) point of intersection of the low frequency end of the semicircle with the Z' axis. Then Rb was used to evaluate the ion conductivity of the samples according to the expression

$$\sigma = t \div (A \times R_B) \qquad (1)$$

where in our case $t=150~\mu m$ was the thickness of the examined electrolyte films. The effective electrically-active area of the samples was $A=0.75~cm^2$ (the contact area of the electrodes).

Thus, from the data in Fig. 18 a, b, we estimated σ of PEO/PVP/NaIO₄/TiO₂ NCSPEs. Up to 3 wt% concentration of TiO₂ NPs, σ increases with the increasing concentration of TiO₂ NPs and reaches a value of 1,6 x 10⁻⁶ S.cm⁻¹ at ambient temperature (Fig. 18 b). As compared to undoped PEO/PVP/NaIO4 SPE, the enhancement of is by a factor of 12.

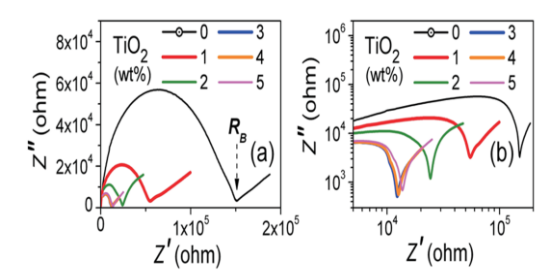


Figure 18. Nyquist complex impedance plots for PEO/PVP/NaIO₄/TiO₂ NCSPE with TiO₂ NPs at various concentrations (according to spectra given in Fig. 17), in linear (a) and logarithmic (b) scale;

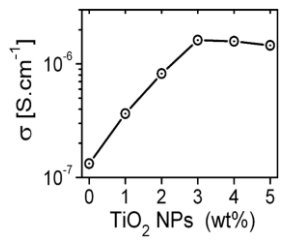


Figure 19. The variation of room-temperature ionic conductivity of PEO/PVP/NaIO₄/TiO₂ NCPEs versus the concentration of TiO₂ NPs

As for the TiO_2 -produced increase in σ , it results from the synergetic effect due to interfacial interactions between the organic functional units of both polymers in the

semicrystalline PEO/PVP polymer blend, on the one hand, and TiO₂ NPs on the other. These interactions are due to the surface of the nanoadditives (promotion of conducting path at the surface of the NPs which favours long-range ion migration). Such effect has been reported for a lot of nanocomposite salt-complexed SPE systems. The interaction between the TiO₂ nanofiller surface and the ether oxygen atoms of PEO chains results in an enhanced dissolution of the NaIO₄ molecules in the NCSPE thereby increases the number of free Na⁺ ions as evidenced for PEO based NCSPEs. The interactions between the nano-TiO₂ and IO₄ anions also promote more free Na⁺ ions in PEO/PVP/NaIO₄. Both processes lead to an increase of σ by the increasing concentration of the TiO₂ NPs. Certainly, a significant role for the enhancement of σ values of such NCSPEs plays the improvement in the amorphicity and flexibility of the network of their polymer matrix owing to high interfacial interactions of the doping NPs with the polymer chains. In turn, this effect leads to an increase in the segmental mobility of polymer chains that will assist fast ion transport because the inter- and intra-chain ion hoping should be supported more efficiently. However, TiO₂ content higher than 3 wt% does not contribute to enhancement of σ by our NCSPE samples, as observed for 4 wt% and 5 wt% TiO₂ (Figure 19). Most probably, a further loading with 10 nm-sized TiO₂ NPs will also degrade the Na⁺ ion-conducting properties of PEO/PVP/NaIO₄/TiO₂ NCSPEs considered here. This can be attributed to enhanced TiO₂-TiO₂ interactions and possible aggregation (clusters formation) of nano- TiO₂ in the NCSPE, leading to a higher crystallinity, less ion-conducting pathways at the surface of the nanofillers, and probably to more immobilized polymer chains. As a whole, a high content of TiO₂ NPs incorporated into the semicrystalline PEO/PVP polymer-blend matrix does result in weaker Na⁺ ion transport, accompanied by a drop in ionic conductivity.

The real part of AC conductivity (σ_{ac}) for the studied PEO/PVP/NaIO₄/TiO₂ NCSPEs (Figure 20) was determined using the frequency spectra of complex electrical impedance by expression

$$\sigma'_{AC}(f) = tZ' \div (A \mid Z \mid^2) \qquad (2)$$

where the parameters t and A are the thickness of the electrolyte films and their electrically-active area, respectively. In our case, $t = 150 \mu m$ and $A = 0.75 cm^2$.

The quantity σ_{ac} describes the macroscopic nature of the electrical conducting process. Physically, σ_{ac} is related to the dissipation of charges and represents dissipation of energy due to dipole or flow of charge carrier (i.e., flow of energy). In the low-frequency region, the behaviour σ_{ac} is related to the accumulation of charge carriers at the electrode/electrolyte interface. Due to electrode polarization in this region, σ_{ac} decreases by decreasing f. The gradual increase of σ_{ac} towards the higher frequencies is usually reported for similar category ion-conducting SPE systems.

Such behaviour signifies the increment of displacement currents owing to attenuation of capacitive reactance. Importantly, the $\sigma^{'}_{ac}$ values of the TiO2- nanofilled PEO/PVP/NaIO4 are higher than those without TiO2 NPs. This is attributed to increased ion conduction paths resulting from the nanoadditives, a fact well known for NCSPEs

and polymer/ TiO_2 nanocomposites. Significantly, it is seen in Fig. 20 that the σ'_{ac} values of PEO/PVP/NaIO₄/TiO₂ increase with increasing TiO₂ content up to 3 wt%. In particular, the plot of σ'_{ac} for PEO/PVP/NaIO₄/TiO₂ at 1 wt% TiO₂ (Figure 20) exhibits two distinct slopes: in the low- and high-frequency regions, respectively. At higher frequencies (>10⁵ Hz), a steeper increase of σ'_{ac} takes place (Figure 20).

Such behaviour of σ'_{ac} has been previously observed by ion-conducting SPEs and NCSPEs, both based on the semicrystalline matrix PEO/PVP. Generally, the high-frequency region of $\sigma'_{AC}(f)$ characteristics might follow Jonscher's power law at a particular temperature,

$$\sigma'_{AC}(f) = \sigma_0 + Cf^n \qquad (3)$$

where C is a constant, n is a power factor (0 < n < 1), and σ_0 is the conductivity at $f \rightarrow 0$. The frequency exponent n may provide information on the mechanism of ion dynamics in different frequency regions, such as free and correlated hoppings. The above frequency-dependent conductivity function is the so-called universal dielectric response. It is typical for heterogeneous systems and disordered materials and is widely displayed by conducting polymer networks and polymer electrolytes. At $f < 10^5$ Hz, the frequency-dependent conductivity of considered NCSPE systems at a concentration of TiO₂ NPs 2-3-4-5 wt% satisfy the Jonscher's power law. However, at higher frequencies $(f > 10^5 \text{ Hz}) \ \sigma'_{ac}$ was observed to diminish by increasing frequency f (Figure 20).

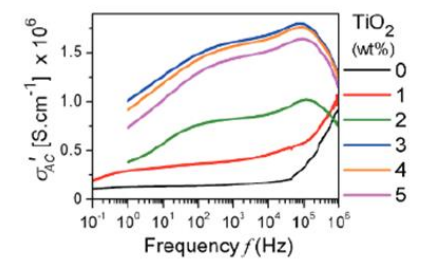


Figure 20. Real part of AC conductivity σ'_{ac} vs. frequency f.

4.1.2. Polymer electrolyte PEO/PVP/NaIO4/GO

As evidenced by SEM studies, the surface of pure blend electrolyte (Figure 21(a)) was found to be relatively rough and composed with micro-voids and cracks, which signifies the crystalline nature. The formation of micro-voids at film surface is due to rapid evaporation of the solvent during the preparation of polymer blends. Apparently, surfaces of the blend electrolyte films become smooth upon increasing of complexing salt concentration as shown in figure 21b. This indicates the increase in

percentage of amorphous portion in the matrix of blend electrolytes due to random distribution and dissociation of salt. Significantly, the GO doped salt complexed polymer electrolytes demonstrated relatively smoother surface topology (Figure 21(c)), it can be attributed to enhanced portion of amorphous region in the matrix of resultant salt complexed blend electrolyte due to addition of Graphene oxide.

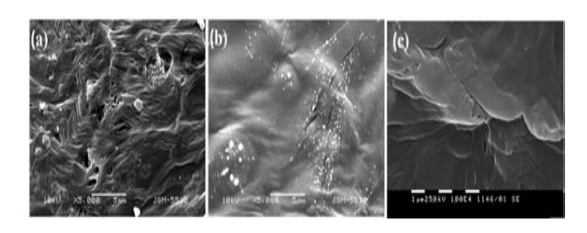


Figure 21. SEM images of NaIO₄ salt complexed and GO doped PEO/PVP electrolytes: a) PEO/PVP blend, (b) PEO/PVP/NaIO₄ (10 wt%), (c) PEO/PVP/NaIO₄ (10 wt%)/GO (0.4 wt %)

Figure 22 represents XRD patterns of pure blend (PEO/PVP) and its complexes with NaIO4 salt at different concentrations and GO (0.4 wt%) doped 'PEO/PVP/NaIO4 (10 wt%)' blend electrolytes. The diffraction pattern of pure blend (PEO/PVP) displays intensity diffraction peaks at 2 θ =19.30 and 2 θ =23.40 (figure 22(a)) corresponding to characteristic crystalline peaks of PEO, which originates from the ordering of polyether side chains and strong intermolecular interaction between PEO chains through the hydrogen bonding [14]. The gradual decrease in intensity and increase of broadness of the diffraction peaks as a function of complexation of NaIO₄ salt (figure 22 (b) - (d)), reveal the decline in crystalline nature of blend electrolytes. This could be due to strong interaction of dissolved NaIO₄ salt with host polymer matrix and intermolecular interaction among the polymer chains of blend electrolytes, which lead to increase of amorphous phase in polymer blend electrolytes. It is seen that (as evidenced from figure 22 e) the intensity of characteristic XRD peaks corresponding to PEO further decreased by doping of 0.4 wt% of GO to 'PEO/PVP/NaIO₄ (10 wt%)'electrolyte system. This evidences for further increase of amorphous portion in salt complexed electrolytes by the addition of GO, which favors the enhancement of mobility of the mobile charge ions in the polymer electrolytes and leads to an increase in the ionic conductivity.

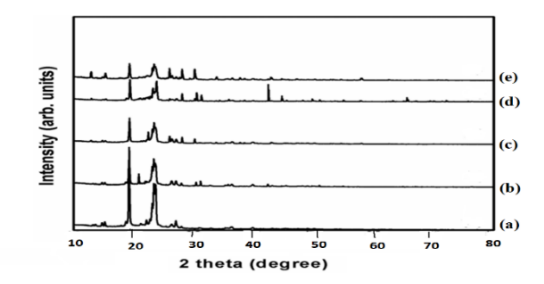


Figure 22. XRD spectra of pure, NaIO₄ complexed and GO doped PEO/PVP blend electrolytes:(a) PEO/PVP pure blend, (b) PEO/PVP/NaIO₄ (5 wt%), (c) PEO/PVP/NaIO₄ (7.5wt%), (d)PEO/PVP/NaIO₄ (10wt%), (e) PEO/PVP/NaIO₄ (10 wt%)/GO(0.4 wt%).

Figure 23 illustrates the variation in electrical conductivity of pure, salt complexed and GO doped polymer blend electrolytes as a function of temperature in the range 303–343 K. Evidently, the linear variation of resultant curves represents Arrhenius type of thermally activated process by satisfying the following equation:

$$\sigma_{dc} = \sigma_0 \exp(-E_a \div KT) \quad (4)$$

where σ_0 , E_a , K and T represent the pre-exponential factor, activation energy, Boltzmann constant and absolute temperatures, respectively.

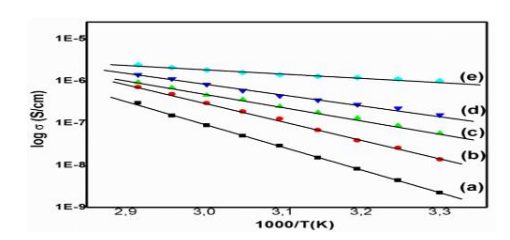


Figure 23. Arrhenius plots for NaIO₄ salt complexed and GO doped 'PEO/PVP blend' electrolytes: (a) PEO/PVP pure blend, (b)PEO/PVP/NaIO₄ (5 wt%), (c) PEO/PVP/NaIO₄ (7.5 wt%), (d)PEO/PVP/NaIO₄ (10wt%), (e) PEO/PVP/NaIO₄ (10wt%)/ GO(0.4 wt%).

Figure 24 reports the frequency spectra of the real (Z') and imaginary (Z'') parts of complex electrical impedance of the studied GO/PEO/PVP/NaIO₄ nanocomposites, and Figure 25 presents the corresponding Nyquist plots (complex impedance plane diagrams, Z'' vs Z'). For all our samples, the Nyquist plots demonstrate well-defined semicircles attributed to the presence of parallel combination of bulk resistance and bulk capacitance. The ionic conductivity (σ) of the samples was calculated according to the

relation (1), where t and A are the thickness of the sample and the area of the electrodes (i.e., the electrically-active area of the electrolyte film), respectively. R_B is the bulk resistance of the samples. Intercept of the low-frequency spike at the Z' axis of the Nyquist plot gives the value of R_B .

Figure 26 shows the values of σ for GO/PEO/PVP/NaIO₄ as depending on the concentration of incorporated GO. Up to 0.6 wt.% content of GO, σ is increasing with increasing concentration of GO and reaches value of 3 × 10⁻⁶ S/cm at 0.6 wt.% GO. As compared to GO-free PEO/PVP/NaIO₄ electrolyte, this is an enhancement of about 20 times.

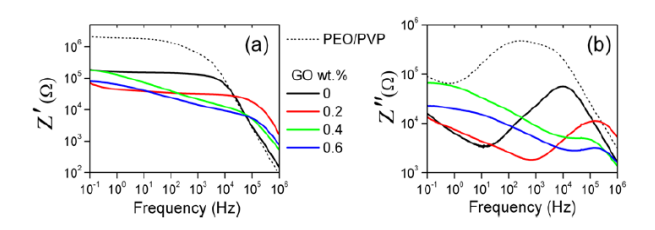


Figure 24. The frequency spectra of the real (Z') and imaginary (Z'') parts of complex electrical impedance of the studied GO/PEO/PVP/NaIO₄ system composed with nanosized GO incorporated at concentrations 0; 0.2; 0.4 and 0.6 wt.%. The impedance spectra of PEO/PVP blend at the same compositional ratio (PEO:PVP = 70:30 wt.%) are also given for comparison (dashed lines). All spectra were recorded at room temperature at the same experimental conditions.

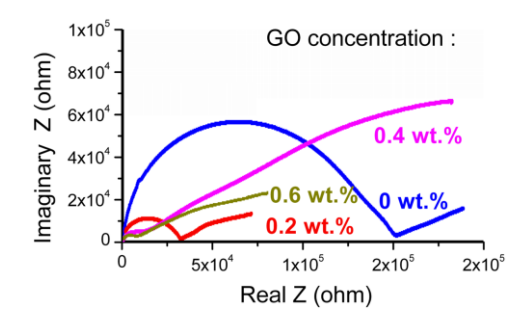


Figure 25. The Nyquist complex impedance plots for GO/PEO/PVP/NaIO₄ at various concentration of GO

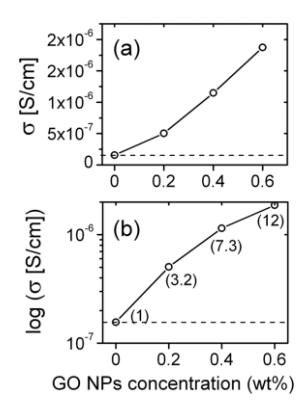


Figure 26. The values of conductivity σ of GO/PEO/PVP/NaIO₄ as a function of the concentration of incorporated GO

The spectra of the real (ε') (figure 27a) and imaginary (ε'') (figure 27 b) parts of the dielectric permittivity calculated from their impedance data.

$$\epsilon' = -\frac{z''}{\omega C_0 \left(z'^2 + z''^2\right)} \quad (5)$$

$$\epsilon'' = \frac{\mathbf{z'}}{\omega C_0(\mathbf{z'}^2 + \mathbf{z''}^2)} \qquad (6)$$

where C_0 is the vacuum capacitance ($C_0 = \varepsilon_0 A/d$; $\varepsilon_0 = 8.85 \times 10^{-12}$ F/m is the permittivity of free space), $\omega = 2\pi f$ is the angular frequency, where f is the frequency of applied electric field. The dielectric properties are of interest because they determine the ability of the dielectric material to store electrical energy. ε' is the lossless permittivity that represents the ability of the dielectric material to store energy during each charging cycle and returned to the electric field at the end of the cycle. ε'' represents the dielectric loss (the energy dissipated by conduction).

It is known that the increase of dielectric permittivity at low frequency is related to the electrode polarization effect, which occurs due to the formation of electric double layers that are built up by the free charges at the electrolyte/electrode interface [15]. In our case, most important is that the GO-doped PEO/PVP/NaIO₄ exhibits a considerably enhanced dielectric response as compared of GO-doped PEO/PVP/NaIO₄ over given frequency ranges can reach a factor of 60 and 12, respectively, as compared to the undoped PEO/PVP/NaIO₄ electrolyte.

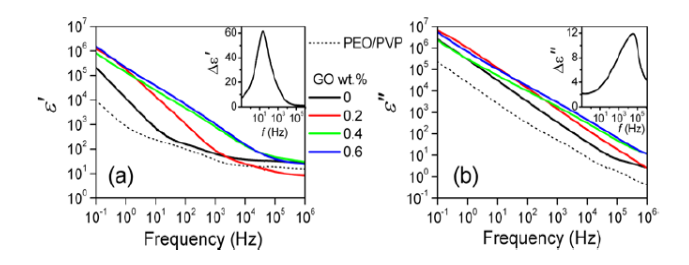


Figure 27. (a) The frequency-dependent real (a) and imaginary (b) parts of the dielectric function of GO/PEO/PVP/NaIO₄ NCPEs containing 0; 0.2; 0.4 and 0.6 wt.% GO nanofillers. The spectra of the dielectric function of PEO/PVP blend at the same compositional ratio (PEO:PVP = 70:30 wt.%) are also given for comparison (dotted lines). The inserts: the frequency-dependent increment of the dielectric function $\Delta \varepsilon'$ and $\Delta \varepsilon''$ (see the text).

4.2. Investigation of composites and nanocomposites based on liquid crystals

4.2.1. Investigation of a nanocomposite of nematic liquid crystal E7 and graphene

One of the most widely known applications of the nematic liquid crystals

(LCs), namelly in thin-film-transistor LC displays (in digital cameras, various monitors and large-screen high-definition television sets), has given evidence that the ions in these electro-optical materials impact the image quality due to the ionic shielding phenomenon [16, 17]. That is why, the development of novel LC-based composite materials is an exciting challenge for investigation in order to solve this problem. In recent years, important direction of the research work was the modification of the properties of LCs by doping with different nanoparticles (metallic, semiconducting, ferroelectric) in order to obtain improved electro-optical characteristics. It has been demonstrated that a very small amount of nanoparticles can strongly modify the dielectric, elastic and electro-optical properties of the host LC [18, 19]. Among various nanoparticles, graphene is the carbon nanomaterial that is most promising for improvement of the electrical properties of the nematics due to its electronic transport properties [20, 21]. In particular, Gökçen et al. have investigated the effect of graphene being doped in LC E7. The results showed that the dielectric and electrical behaviors of the LC E7 are strongly influenced by graphene. Also, it was found that the doping with graphene reduces the electrooptics-relevant threshold voltage of graphene-E7 nanocomposites. In the study presented here, we have examined the electrical response of E7 doped with very low amount of graphene (10⁻³ wt.%). To inspect the effect from graphene, our interest was concentrated on the frequencydependent alternating-current (AC) electrical impedance of

nanocomposite.

Characterization of the samples was performed by modular potentiostat/ galvanostat SP-200 Bio-Logic (Bio-Logic Science Instruments). This compact and powerful computer-controlled instrument for impedance spectroscopy is well suited for precise measurements in the nanotechnology research. Hardware filtering allows removing unwanted electromagnetic noise which can affect the quality of the experimental data.

Figure 28 reports raw data for the complex electrical impedance Z^* measured for considered films of either E7 or graphene-doped E7 as a function of frequency f of the external electric field (in our case, applied perpendicular to the film plane). Due to the same geometrical dimensions of both samples (thickness and electrically-active surface area), it can be made not only qualitative, but also quantitative comparison. As seen, there is some frequency range, namely bellow 1 kHz, in which the impedance of the sample with graphene-doped E7 is higher than that of the sample with pure E7. Notice, the low-frequency measurements give information on electrical conductivity and ionic contributions. The trend of lowering of the ionic conductivity can be seen in the research on nematic E7 doped with graphene at concentration of 0.05 wt.%, as well as for nematic LC 4-cyano-4'-pentylbiphenyl (5CB) doped with graphene at concentration of 0.005 wt.%. Note that in our case the graphene concentration is even less (0.001). Generally, the impedance spectra in Figure 28 can be further analyzed and both AC and direct-current (DC) conductance may be exactly calculated by applying suitable theoretical model, e.g., through the corresponding frequency spectra of the complex dielectric permittivity and their fits. But the main result for the effect from graphene nanodopants is visible even from the electrical impedance data [22 - 25].

The effect of graphene nanoparticles can be clearly seen in the Nyquist plots (the imaginary part versus the real part of the impedance) of our LC samples (with or in the absence of graphene). Fig. 29 shows the corresponding impedentiometric response of both samples to be compared. The Nyquist plot consists of a part of semicircle towards higher frequency side, followed by a steep line at lower frequency side. The semicircle represents the bulk material (such shape is relevant to equivalent circuit of capacitance and resistance connected in parallel). The value of the bulk resistance (R_B) of the material can be determined from the point of intersection of the high-frequency end of the semicircle with the Re(Z) axis. It is seen from Figure 29 that compared to the reference cell made with pure E7, the graphene-doped E7 exhibits higher R_B . According to the simplified expression (1), where t and t are the thickness and effective electrically-active area of the examined LC films, respectively, from the data in Figure 28 one can roughly estimate that the conductivity t0 for our sample with graphene-doped E7 is nearly twice lower than the one of the reference E7 sample.

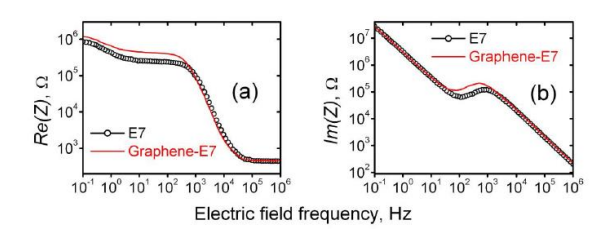


Figure 28. Data obtained by impedance spectroscopy: (a) real and (b) imaginary parts of complex electrical impedance measured for the samples with: E7 (open circles); graphene-doped E7 (solid lines). The temperature of the films was 26° C

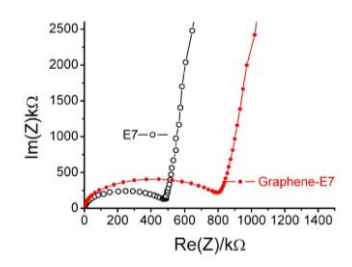


Figure 29. Nyquist complex impedance plots for the samples under study (relevant to data given in Figure 28).

Nanodoping by small amount of graphene is currently trending nanotechnology to largely improve the properties of liquid crystals LC (LCs), in particular their electrical and electro-optic responses. In the study presented here, we used thin (7 $\mu m)$ planar films of nematic LC E7 doped with $10^{\text{-}3}$ wt.% graphene nanoparticles.

In order to assess the effect from this small amount of graphene doping, we compared the electrical and dielectric response of such nanocomposite nematic films with that of the same LC E7 but undoped. The study is in the area of /material nanoscience and nanotechnology, and is closely related to practical applications of nematic nanomaterials. By the technique of complex electrical impedance spectroscopy, both real (Zr) and imaginary (Zi) parts of the complex electrical impedance (Z*) were simultaneously measured as a function of the frequency (f) of the AC electric field applied on the sample. The Nyquist plots (Zi versus Zr) for the studied samples demonstrated semi-circular arcs (Figure 31a). The deep valleys in these plots are associated with the bulk resistance (Rb) of the samples. The Rb values can be associated to the projections of the valleys on the abscissa (Zr axis). As seen at Figure 31(a), Rb of our thin planar films with graphene-doped E7 is approximately twice higher than Rb

of such films with pure E7 and this applies to any temperature in the range $15^{\circ}C - 60^{\circ}C$ (Figure 30) [26].

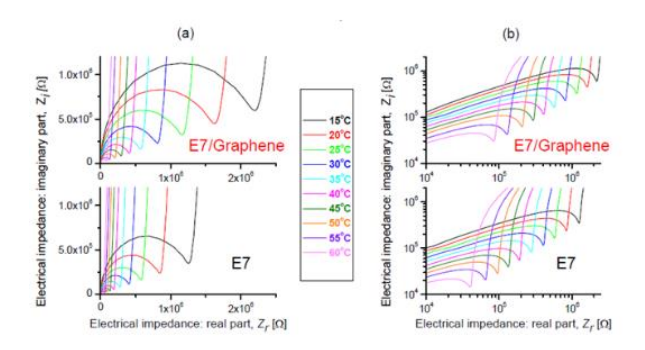
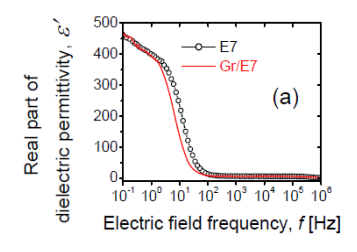


Figure 30. The complex Nyquist plots for planar films of graphene/E7 nanocomposite and undoped E7, measured upon identical experimental conditions, but at various temperatures; (b) The same as in (a) but in logarithmic scale

In fact, a clear difference between the graphene/E7 nanocomposite and the undoped E7 was also present in their dielectric spectra (figure 31). The real (ϵ') and imaginary (ε") components of the complex dielectric permittivity were calculated from the measured frequency spectra Zr(f) and Zi(f) by means of the well known relations (5) and (6), where $\varepsilon_0 = 8.85 \times 10^{-12} \, \text{F.m}^{-1}$ is the permittivity of free space. ε' has the same significance as that of the ordinary dielectric constant of the material. It is a measure of the energy stored in the material during each cycle, to be returned to the electric field at the end of the cycle. The high values of ε' in the low-frequency region $(f < 10^2 \text{Hz})$) can be attributed to a build-up of space charge near electrode/LC interface, which partially blocks the charge transport. With increasing f, ε' decreases up to a nearly constant value, because at such frequencies the ions will hardly able to follow the periodic reversal of the electric field. Significantly, graphene-doped E7 exhibits a lower value of dielectric constant ε' than the undoped E7. This difference is most pronounced in the low-frequency region, in our case from 1 Hz to 100 Hz. As known, in this range the dielectric behavior is attributable to the space-charge polarization, i.e. the addition of graphene nanoparticles to the ion-rich nematic host E7 effectively leads to capturing of mobile ions and reducing of the space-charge polarization. The decrease in the dielectric constant represents a fractional decrease in charge density due to the addition of graphene nanoparticles in the LC E7, resulting in a lower ion conductivity.



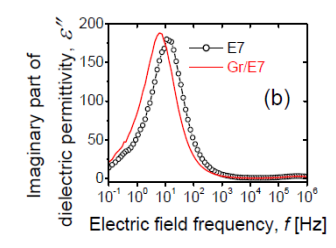


Figure 31. The frequency spectra of the real (a) and imaginary (b) parts of the complex dielectric permittivity function ε^* for planar films of graphene/E7 nanocomposite and undoped E7 measured at 26° C and identical other experimental conditions.

Our study shows that the electrical and dielectric behaviours of planary-aligned thin films of nematic LC (E7 in the present case) are influenced by its doping with graphene nanoflakes, even at very low concentration of 10^{-3} wt.%. Essentially, the results obtained here confirm the concept that the doping with graphene nanoparticles reduces the ion diffusivity, and thereby, lowers the room-temperature electrical conductivity of the doped nematic LCs. This applies to the ionic conductivity (relevant to the low frequencies) (and direct-current conductivity), as well as to AC conductivity in certain frequency range (in our case, 10 Hz - 10 kHz).

Slight amounts of graphene nanodopants reduce the concentration of impurity and injected ions and their diffusivity, thus depressing the unwanted ion-charge effects in the nematic LCs. The ion immobilization effect through graphene nanoparticles is well pronounced. As such, it will be useful in view of practical applications of nematic nanocomposites produced from graphene-doped nematic LCs (e.g., as EO materials in high-quality LC display technology).

4.2.2 Investigation of polymer-liquid crystal composites (PEO/E8)

In recent years, the (polymer/liquid crystal (LCs)) composites (PLCCs) have attracted great research and application interest due to their unique electrical, dielectric, mechanical, and thermal properties [27 - 31]. In particular, such materials have found wide use in the polymer-dispersed LCs (PDLCs) technology for electro-optical devices and smart windows, well developed at present. Various kinds of advanced multifunctional PLCCs engineered by use of nematic liquid crystals (NLCs) , have been extensively studied in view of their practical use in soft organic electronics and sensorics, as well as in the field of rechargeable mini-batteries.

It is well known that the increasing the amorphous portion in PLCCs is a key factor for enhancement of their ion conductivity. For such purpose, in 2016 Alexander G. Petrov suggested a promising approach, based on the ability of LCs to form glassy

state. In general, glassy state formation in LC systems can be provoked by varying the concentration of the LC additives. Further, there are evidences that the coupling of LCs to the polymer network in this case leads to increase of viscosity of the PLCCs.

Thin films of PEO/E8 PLCCs attracted our interest because they exhibit electrical properties that are of importance for molecular electronics and soft-electronics applications.

The synthetic polymer poly(ethylene oxide) (PEO) is often used as a polymer matrix in polymer-salt composites' electrolytes. PEO is a semi-crystalline material with flexible ethylene oxide segments. At ambient temperature, PEO exhibits sufficient chain flexibility, and the semi-crystalline structure of this polymer makes it suitable as a host for alkali metal ions and supports ionic conductivity. PEO-based polymer electrolytes are among the most promising materials due to their good thermal properties and interfacial stability with metal electrodes. The low glass transition temperature (Tg) of PEO, as well as its flexibility and other valuable properties, are well suited for engineering composite materials made from PEO and mesogens. The research interest in polymer-LC materials is driven by the possibility of forming flexible electrolyte membranes with enhanced response and functionality. Due to the improved electrical properties, various electrolytic polymer-LCs molecular systems based on polymer PEO have been synthesized and investigate. New fields of development and application of such polymer electrolytic materials are challenging scientific research areas, and many studies are focused on this. In particular, novel electrolyte materials with microscopic porosity are attractive for fundamental research and industrial applications. Previously, flexible polymer/LC composites from PEO and the LC mixture with the commercial name E8 were synthesized, and thin films of PEO/E8LC were investigated. The wellknown room-temperature nematic E8 is a eutectic mixture of LC cyanobiphenyl derivatives and cyanoterphenyl LCs. E8LC is characterized by high chemical and thermal stability, a wide temperature range of the nematic phase, relatively large dielectric anisotropy, as well as proper elastic constants and viscosity.

PEO/E8 composites have great potential as a platform for producing electrolytes and other functional materials for sensorics and organic electronics applications. Compared to pure PEO, these composites were found to have considerably enhanced electrical conductivity and dielectric permittivity, which can be tailored by their phase-separated morphology. Further, PEO/E8/NaIO₄ Na⁺ ion-conducting polymer-LC electrolytes were synthesized and examined - they demonstrated excellent ion electrolytic and dielectric properties, and hence, are attractive for diverse applications. In the PEO/E8 and PEO/E8/NaIO4 ion conductors, an intermolecular coupling between PEO and E8LC was suggested. In the present study, the frequency spectra of complex electrical impedance and dielectric permittivity of thin films of these composites were analyzed depending on the temperature in the vicinity of their glass transition — a situation in which the dipole contribution to impedance and dielectric response can be well sensed. The study of dipole polarization and dielectric relaxations in the inspected PEO/E8-based ion-conducting polymer/LC composites and their temperature dependencies is directly related to the practical applications of the thin

films of these advanced materials. To elucidate on the role of the embedded LCs, the temperature-dependent dielectric properties of both PEO/E8 and PEO/E8/NaIO $_4$ were compared.

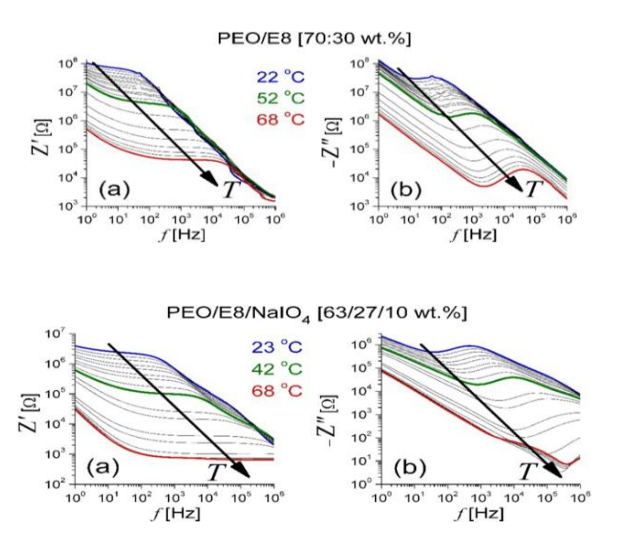


Figure 32. Frequency spectra of complex electrical impedance (real (a) and imaginary (b) parts) of PEO/E8 (70:30 wt. %) and PEO/E8/NaIO₄ (63:27:10 wt.%)

Figure 32 reports the couples of frequency spectra of the real (Z') and imaginary (Z") parts of Z* of the PEO/E8 composite film, simultaneously measured as a function of the frequency f of the AC electric field applied to the film at gradually elevating temperature in twenty equal steps within the temperature range of 22°C – 68°C. The impedance behaviors were of relaxation type. In particular, each of the Z' (f) spectra displayed a pair of a broad minimum (at lower f) and one broad peak (at higher f), both related to typical dielectric relaxation in dielectric media. It is known that the minimum in Z" (f) spectrum is related to the electrode polarization effect, i.e., the accumulation of charges in the electrode-electrolyte interface and the formation of an electric double-layer. The presence of a double-layer (electrode polarization) strongly affects the observation of the dielectric relaxation processes. In general, the relaxation phenomena are controlled by free-volume-activated kinetics or by thermally activated kinetics. The maximum of Z "corresponded to the main dielectric-active relaxation that occurred in the dielectric materials under the action of an external AC electric field (i.e., by induced electric polarization). The frequency of the Z "peak (fmax Z"), known as the relaxation frequency, defined the characteristic relaxation time $\tau = (2_{\text{max}} Z^{"})^{-1}$ of the medium.

In general, using experience found in previous investigations of such media studied by EIS, one can accept that this peak originates from the orientation of dipoles (dielectric relaxation of the orientational electric dipole polarization). From Figure 32 b, it is possible to observe that the gradually increased temperature of the studied polymer -LC composite led to a shift of fmax Z "(together with the frequency of the minimum in the Z "spectra) towards higher frequencies, from 50 Hz (at 22 C) to 40 kHz (at 68 C). The observed shift resulted from dielectric relaxation and was due to the decrease in the dielectric relaxation time. By comparison with the Z spectra of the two ingredients of the PEO/E8 composite, PEO and E8LC measured under the same experimental conditions, it is clear that the effect from the embedded E8 LC molecules was significant and resulted in impedimetric and dielectric relaxation behaviors that were intermediate between those of the polymer and the LC.

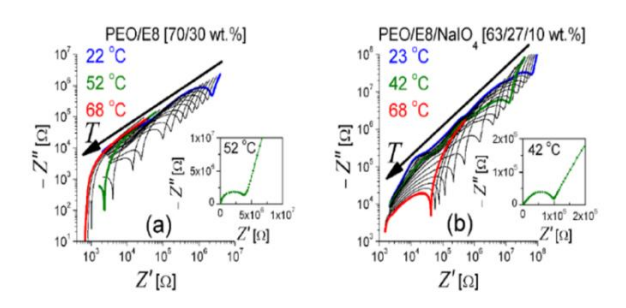


Figure 33. Nyquist plots of PEO/E8 u PEO/E8/NaIO4 at various temperatures.

The above results of the thermal behaviors of PEO/E8 and PEO/E8/NaIO₄ can be highlighted by the presentation of the temperature-dependent $\{Z', Z''\}$ spectra of these composites by means of the corresponding complex impedance diagrams- the Nyquist plots (Z'' versus Z'). They consisted of semicircle arcs on the high-frequency side, followed by a steep line on their low-frequency side (Figure 33). The semicircle corresponded to bulk material properties (such shapes are relevant to the equivalent circuit of capacitance and resistance connected in parallel). In the lower-frequency region, the gradual increase in absolute Z'' values as the frequency decreases indicated a build-up of electric double-layer capacitance at the electrode/electrolyte interface. The value of the bulk resistance (R_B) of the material could be determined from the point of intersection of the low-frequency (i.e., high-resistance) end of the depressed semicircle on the Z' axis. Then, the values of the ion conductivity of the studied composite films were obtained from R_B .

The $\{Z', Z''\}$ behaviors of the PEO/E8 composite, as well as their temperature change, suggested a dipolar molecular organization in this polymer/LC system. In our case, the dielectric relaxation may typical dipole reorganization in the PEO/E8

composite caused by applying an external AC electric field. The relaxation in the dielectric PEO/E8 upon the AC field was related to the contributions of both the polymer chains of PEO and the LC soft matter. Coupled molecular dipoles are possible in such polymer/LC composites. Intermolecular PEO-E8LC formations owing to functional groups of both PEO and E8 LC have been evidenced by microstructural investigations of the studied PEO/E8 composite. PEO-E8LC intermolecular coupling may have occurred due to electric dipole—dipole interaction between the LC molecules of E8 and PEO oxygen in the structural units of PEO (Figure 34). Cyano compounds in E8LC promoted PEO-E8LC interactions since they had highly polarized cyano groups and easily polarizable biphenyl groups. The cyano end group in the chemical structures of the E8LC molecules was strongly electron-withdrawing, while the oxygen atoms in the [-CH2-O-CH2]n backbone structure of PEO were electron-donating. The C-O-C bond in the ether functional group of PEO was polar (slightly polar). The polar molecular configurations in PEO/E8LC composite can be considered as coupled dipoles formed from single or more LC molecules of nematic E8 with ether oxygens in the C-O-C subunit of PEO, in the process of synthesis of the composite. The finite relative displacement of positive and negative charges produced composite dipolar molecular formations in PEO/E8LC throughout a given spatial volume in which these charges were present. The strong interactions between PEO polymer chains and dispersed rodlike molecules of E8LC led, in practical terms, to a coupling of the LC molecules to the polymer backbone, and their electric-field-driven reorientation was strongly hampered. Due to the flexoelectric and flexodielectric properties of nematic LC molecules, the coupled PEO-E8LC molecular dipoles can be further considered as flexodipoles. The impedance data discussed above, and the following results, support such a model of dipolar molecular organization and dipole-dipole interaction in the studied PEO/E8 composite.



Figure 34. Intermolecular coupling of PEO with liquid crystal 5CB

Figure 35 illustrates the Nyquist plots (–Z" versus Z' complex diagrams) for the impedances measured for PEO/E8 composite film at different temperatures. Note that the values of the imaginary part (Z") of the complex impedance of these dielectric materials were negative, i.e., the impedance is capacitive. It is seen from Fig. 35 that the impedentiometric response of the studied PEO/E8 thin films consists of semicircular arc on the high-frequency side, followed by a steep line (forming an inclined spike) at the low-frequency side. The centre of the depressed semicircle lies on the Z'-axis. The semicircle corresponds to the bulk electroconducting properties of the sample. Such a shape is relevant to the equivalent circuit of capacitance and resistance connected in parallel. In the low-frequency region, the steep increase of Z" values as the frequency decreases is relevant to a build-up of electric double-layer capacitance at the electrode/sample interface (a phenomenon known as electrode polarization effect of accumulated interfacial charges and permanent/induced polarization).

The value of the bulk resistance (R_B) of the material was determined from the point of interception of the low frequency end of the semicircle with the Z'-axis. Then R_B was used to evaluate the electrical conductivity (σ) of the PEO/E8 composite film according to the expression (1) , where in our case t = 150 μ m was the thickness of the film, and $A=0.75~cm^2$ was the contact area of the copper electrodes. Thus, from the data in Fig. 35 a, b we found that σ of PEO/E8 exponentially increases with the increasing temperature, namely from 3.1×10^{-6} S/cm (at 25 °C) to 3.3×10^{-5} S/cm (at 50 °C) (Figure 36), in accordance with results obtained for similar PLCCs (linear-chains polymers and similar NLCs, such as highly polar cyanophenyls . As established in [32], the E8 NLCs act as a pathway for the movement of the electric charges (ions). The observed temperature-induced enhancement effect agrees with the results from other studies on thin films of PLCCs in the same temperature region 25–50 °C . The increasing trend can be explained in terms of a thermallyactivated hopping transport model.

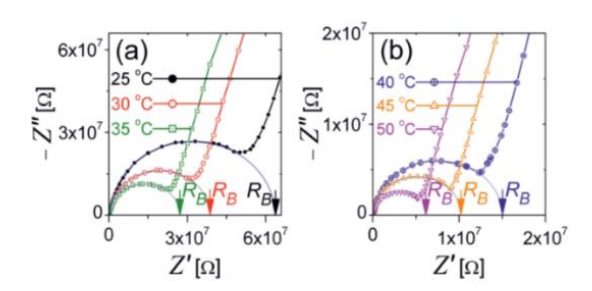


Figure 35. Nyquist complex impedance plots for PEO/E8 composite film at various temperatures

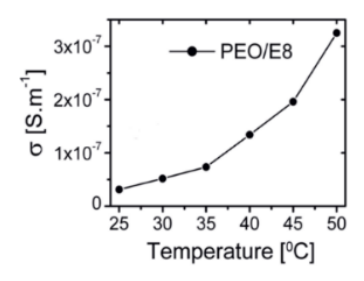


Figure 36. The ionic conductivity (σ) of PEO/E8 film as a function of: temperature

As it was viewed by optical microscope, the studied PEO/E8 FPLCC films display morphology comprising both polymer phase and liquid-crystalline nematic phase. Being entrapped within the bulk of the polymer PEO, distinct microsized LC domains and multi-domains of various sizes, relevant to the LC phase dispersed throughout the polymer system, can be observed (Figure 37). Macroscopically, the LC formations are relatively homogeneously distributed within the volume of the PEO/E8 film. Similar phase-separated mixed polymer-LC morphology [33-36]. It could be suggested that the LCs may be located also in the pores of the polymer PEO, similarly to the NLCs confined in micropore material structures. In fact, the microscopic porosity and microvoids of the studied PEO/E8 FPLCCs, was evidenced by scanning electron microscopy (SEM) studies. The optical anisotropy introduced by the addition of E8 NLCs was observed under polarizing optical microscopy. At a microscale, the nematic LC formations in the PEO/E8 films have random orientation. It should be noted that the observed morphology of the microstructure of mixed polymer and LC phases of the studied PEO/E8 thin films remains the same regardless of temperature of the films (in our case, varied between 25° C and 50 °C).

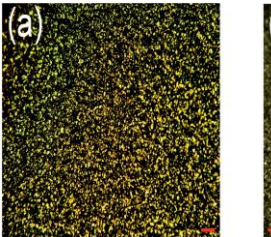




Figure 37. Optical micrographs taken at room temperature (25 °C) for a 150 μ m-thin film of the studied PEO/E8 composites: (a) between crossed analyzer and polarizer; (b) no polarizers. The scale bar is 100 μ m

By using the expressions (5) and (6) and the measured Z and Z spectra, we calculated the real and imaginary parts of the complex dielectric function of the both PEO/E8 (Figure 38) and PEO/E8/NaIO4 (Figure 39) composites under study.

The dispersion curves for both ϵ' and ϵ'' had relaxational characteristics. At a given temperature, the sharp increase in dielectric permittivity at low frequency was related to the electrode polarization, which occurred due to the formation of an electric double layer. In AC fields, the deposed charges forming dipoles at the electrodes led to relaxation behavior that was similar to dipolar relaxation, and the dielectric displayed non-Debye behavior. The non-linear decrease in both the ϵ' and ϵ'' values towards the higher frequency of the applied AC electric field resulted from the contributions of various polarization processes.

It is possible to observe in Figures 38 and 39 that by increasing temperature , the values of both ϵ' and ϵ'' for the two polymer-LC composites were increasing throughout our frequency window. The increases in both ϵ' and ϵ'' could be because the increase in temperature favored the orientation of the molecular dipoles upon the applied electric field that could polarize each separate molecule and the dielectric medium as a whole. Further, Figures 38 and 39 show that by gradually increasing the values of T, there were obvious temperature thresholds equal to corresponding Tg values of the composites. Below Tg, both ϵ' and ϵ'' were slowly increasing functions of T, but at T > Tg, an enhanced dielectric response was present. Moreover, the heating did result in considerable changes in the spectral behaviors of dielectric permittivity. In particular, the change of dielectric loss (ϵ'') values with T signified dipole relaxation and a decrease in the dielectric relaxation time. As a whole, the frequency response of dielectric permittivity of the studied composites agreed with the data reported in the literature for the dielectric response of solid dielectrics and polymer-based solid electrolytes below and above the glass transition temperature.

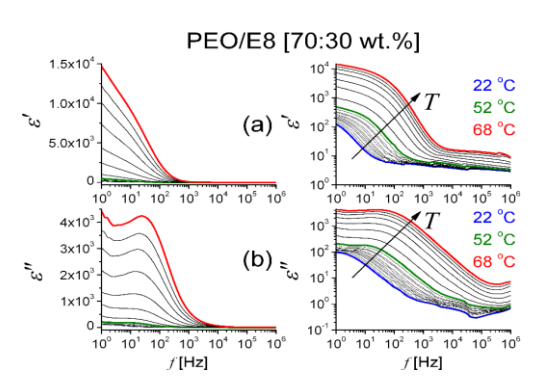


Figure 38 Frequency spectra of complex dielectric function (real (a) and imaginary (b) parts) of PEO/E8 (70:30 wt. %).

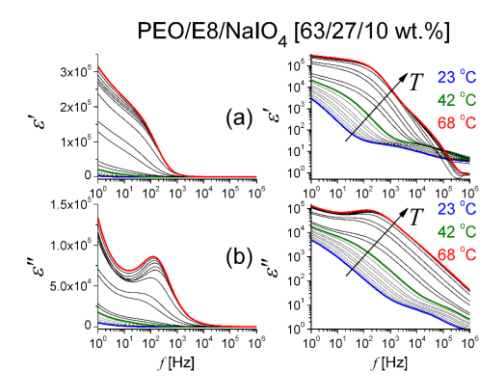


Figure 39. Frequency spectra of complex dielectric function (real (a) and imaginary (b) parts) of PEO/E8/NaIO 4 (63:27:10 wt.%).

4.3. Investigation of LB films

4.3.1. Detection of heavy metal ions by a newly designed biosensor

Nowadays, analytical technologies for water monitoring are well developed to meet the high demands of public health protection [37]. As the quality of drinking water is of paramount importance for human health, great attention, much effort and much research are devoted to improving the detection of contaminants (inorganic and organic chemical compounds, bio-objects, nanoparticles, heavy metal atoms/ions, etc.) that can cause infections and diseases [38]. The EU Drinking Water Directive [39] defines new important parameters that must be monitored to protect human health, with regard to contaminants such as heavy metals, perfluorinated compounds, some types of endocrine disruptors and nanoparticles. In particular, cadmium (Cd) in drinking water is harmful as it can lead to a number of chronic diseases (e.g. cancer and cardiovascular diseases) [40, 41], among other negative health effects [42-44]. This is an ongoing problem in industrialized countries, but increasingly also in low- and middle-income countries. Therefore, knowledge of Cd detection methods and corresponding sensor devices is of particular interest. There are numerous techniques for detecting contaminants at very low concentrations in water, e.g. conventional instrumental analysis (laboratory analysis), microfluidic devices, spectroscopic approaches, plasmonic sensing, etc. [45-49]. As a powerful alternative to conventional analytical techniques for monitoring water quality, biosensors can also provide suitable and highly sensitive detection of contaminants in water. Biomolecules have the potential to be used for sensitive physicochemical detection due to their high selectivity and unique properties. Due to such practical application, we focused our attention on lipid-based systems. Figure 40 presents exemplary frequency spectra of complex electrical impedance (Z) measured for the studied DPPE-NBD LB films deposited on a conductive ITO-glass plate. For the imaginary part (ImZ) of Z, the effect of the presence of Cd^{2+} ions is apparent at high frequency (>1kHz)—the Cd^{2+} ions lead to a decrease of the value of ImZ (Fig. 40b). The same applies to the real part (ReZ) impedance spectra in a broader frequency range spanning almost 5 orders of magnitude (Fig. 40b). In contrast to ImZ spectrum (Fig. 40b), Cd^{2+} ions lead to a change of ReZ within the overall range covered by our apparatus (Fig. 40 a).

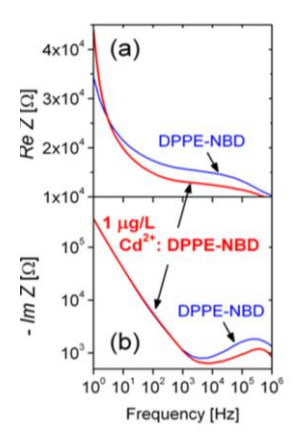


Figure 40. Frequency spectra of real (ReZ) (a) and imaginary (ImZ) (b) parts of complex electrical impedances measured for DPPE-NBD LB films: undoped (thin blue lines); doped with Cd^{2+} ions at concentration $1\mu g/L$ (bold red lines). The measurements were done under identical experimental conditions. The temperature of the films was $25^{\circ}C$.

Well pronounced and indicative is the behavior of ReZ in the low-frequency region (Fig. 41) where the Cd²⁺ ions give rise to increase of ReZ values. Thus, the presence of Cd²⁺ ions results in a significant change (increase) in the slope of the frequency dependence of ReZ in the range 1–10Hz. This can be used to quantitatively analyze the effect from the addition of Cd²⁺ ions the concentration of ions can be estimated using calibrated set of such characteristic curves obtained as depending on several concentrations of Cd²⁺ ions. The analyses of curves' slopes can be used to estimate the effect from Cd²⁺ dopants instead of the estimation of this effect through the decrement of both ReZ and ImZ in the high-frequency range (>1kHz). Note that the considered slope of the frequency dependency of ReZ gives straightforward information and its value does not depend on the absolute values of ReZ. Physically, the increase of this slope in the presence of Cd²⁺ ions is due to the electrical impedance at the interface between the liquid electrode and soft lipid material of the complex dielectric medium

of Cd^{2+} -doped DPPE-NBD. The space charge effects could be thought to be the cause of interfacial resistance. Its role needs to be confirmed by studies of Cd2+ ion-induced interfacial molecular dynamics of the considered phospholipid LB.

Figure 41 shows also the frequency-dependent ReZ measured under the same experimental conditions for identical DPPE-NBD LB film doped in the same way with Cd^{2+} ions, but at twice lower concentration. As seen, the corresponding behavior differs a little from that of undoped DPPE-NBD LB films. This means that the Cd^{2+} concentration of $0.5\mu g/L$ is close to the sensitivity limit of the considered impedimetric detection by the examined phospholipid LB films and measurement configuration presently applied for sensing of these heavy metal ions.

By the deposition of the studied LB films, the Cd^{2+} ions in the water insert themselves between the phospholipid molecules, thus separate them at larger distances. Since DPPE contains a negatively charged phosphate group, an electrostatic interaction (though not very strong) between Cd^{2+} and this molecular system is rather possible. Most probably, Cd^{2+} ions can bind, orient and polarize the carbonyl carbon atom in the phospholipid molecule [38, 39, 50-51].

The presence of the Cd²⁺ metal ions in the liquid subphase could induce changes in the orientational ordering, as well as structural changes in the DPPE-NBD LB monolayer. Moreover, ion-pair formation and complexation are rather possible, which must also be taken into account with a certain degree of importance. Such phenomena can not be directly highlighted by means of impedance/dielectric spectroscopy techniques. More sophisticated investigation techniques should be needed. Detailed analysis of ion-dipole electrostatic interactions forces and the process of electrical conduction in such LB electrostatic assembly (being a mixed soft-solid complex system) is a difficult task. Generally, the capacitance represents the dielectric contribution of the lipid film, and the conductance represents loss processes due to defects, pores, etc. Microdefects such as film contamination, surface defects on the ITO electrode could also have contributions to the measured impedances. In any case, the import of Cd²⁺ ions in the lipid LB monolayer will alter its organization and density, can affect the conformation of the monolayer, which leads to reduction of the very close packing of the DPPE-NBD molecules to each other, as well as to a change of the topological polar surface area of the resultant structural units. This will explicitly result in modification of the anisotropy of both electrical conductivity and dielectric properties of the LB monolayers. Due to the large atomic mass of Cadmium and therefore the small diffusion coefficient, at very low frequencies the ions manage to follow the field and this disrupts the packaging of the LB film that is expressed by the increase of ReZ. This effect is well seen in Figure 40 a and Figure 41. The evidence that DPPE-NBD LB films doped with Cd²⁺ ions at twice lower concentration have practically equal or slightly lower ReZ values than undoped DPPE-NBD monolayer (Figure 41), may indicate a better packaging implementation effect in the former one. By increasing frequency, Cd²⁺ ions are no longer able to follow the external electric field but the induced polarization comes into play which generates a displacement current that manifests itself with a decrease in ReZ. In this case, with respect to undoped DPPE-NBD monolayer the frequency dependence of ReZ for Cd²⁺ -doped LB films is reversed—the higher the ion concentration, the lower the ReZ values (Figure 40 a and Figure 41). This behavior is well observable also in the Nyquist representation of complex impedances discussed in the following.

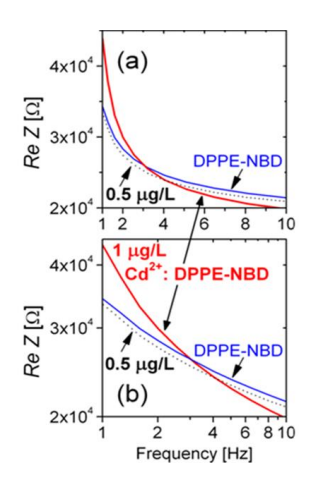


Figure 41. Frequency spectra of real (ReZ) of complex electrical impedances measured for DPPE-NBD LB films, but but in a low-frequency range: (a) linear scale; (b) logarithmic scale

Figure 42 presents the Nyquist plots (ImZ vs ReZ) of the impedance spectra recorded. The semicircle-like shape (relevant to the high-frequency side of impedance spectra) and the steep curve (relevant to the low-frequency side of impedance spectra) in these plots correspond to the electrical conductive properties and electrode polarization effect (EP), respectively. By dielectrics in capacitor-like geometry, the increase of ReZ and ImZ values toward the zero frequency is caused by EP. At low frequencies, this process dominates over the other dielectric polarization processes. EP is an accumulation of long-distance travelled charges at the interfaces between the electrode and the dielectric This depends on the surface topography, chemistry, and area of the electrode, as well as the chemical composition of the sample (the LB film) under analysis. The ReZ value Ric of the interception of both curves (represented by the dip in the Nyquist plot), can be associated with a parameter that is relevant to the electrical conductivity (σ) of the LB film. As seen from Fig. 42, the presence of Cd²⁺ ions in the lipid DPPE-NBD LB monolayer under study results in an increase of its conductivity, according to the relation (1), where t and A represent the thickness and electricallyactive area of the sample, respectively. The increase of the conductance of the lipid NPPE-DNB LB monolayer is a result of its conformational changes due to Cd^{2+} ions. The binding of cationic Cd^{2+} to the lipid polar headgroup renders the lipid surface (partially) positively charged, which might facilitate the transport of anionic electroactive species to the surface of the electrodes. Inconclusion , EIS could be an effective method to analyze and understand the features of phospholipid LB monolayer which surface is modified with heavy metal ions.

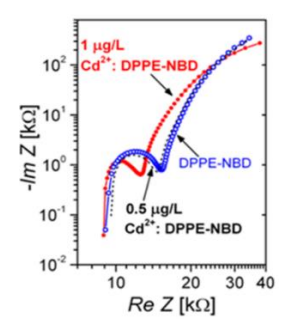


Figure 42. Nyquist complex impedance plots for the studied lipid LB films.

4.3.2. Phospholipid Langmuir-Blodgett films and impedance spectroscopy for the detection of acetone and methanol vapours

Volatile organic compounds (VOCs) belong to a class of reactive gases and vapours that are currently attracting increasing attention. These chemicals have high vapor pressures and evaporate rapidly at room temperature. When released into the atmosphere, they can pose a serious threat to the environment and human health. Methanol is widely used in various industries (organic synthesis, pharmaceutical and plastic industries) for the production of paints, drugs, pesticides, explosives, etc. It is a toxic compound (if ingested) and can cause eye injuries. Its vapours are flammable, explosive and hazardous, especially when inhaled. Measuring VOCs is challenging because they are generally unreactive and have limited affinity for solid surfaces. This makes it difficult to find materials that can selectively bind to or adsorb them. Most of the currently used high-performance analytical methods, e.g. gas chromatography or mass spectroscopy, are laboratory methods for measurement and in-depth analysis. These are difficult to implement in real time, so approaches such as chemical sensors and biosensors are considered as alternatives. Phospholipid layers have great potential to be used for sensitive physicochemical detection and chemical/biochemical monitoring due to their high selectivity and unique properties [52-54]. In particular, Langmuir-Blodgett DPPE-NBD films have great potential for chemical and biological sensing [55]. As is known, the deposition of LB film is one of the best techniques used

to obtain stable organized supramolecular architectures. The Langmuir-Blodgett technology provides precise control of the thickness and molecular orientation, as well as the deposition in a random phase of the layer [56, 57].

Figure 43 and Figure 44 show the frequency spectra of real (ReZ) and imaginary (ImZ) parts of complex electrical impedance Z=ReZ+i ImZ measured for a DPPE LB film studied here upon acetone vapours. As seen, the presence of the vapours of these VOC leads to significant changes of both ReZ and ImZ spectra of the DPPE LB film. The changes are well pronounced in the low frequency region (figure 44) and larger for ImZ spectra. Significantly, at very low frequency (in our case, 0.1 Hz) the measured ReZ clearly shows a decrease of the ohmic resistance (i.e., an increased electrical conductivity) of the studied DPPE phospholipid monolayer in the presence of the vapours of the VOCs detected here. An increase of the concentration of the vapours results in an enhancement of the observed spectral changes. Thus, reduction of the values of both ReZ and ImZ impedances take place for acetone by gradually increasing concentration of vapours. Such changes in the impedance spectra are suitable for quantification of the experimental data obtained at the present level of the concentration of the detected vapours of acetone.

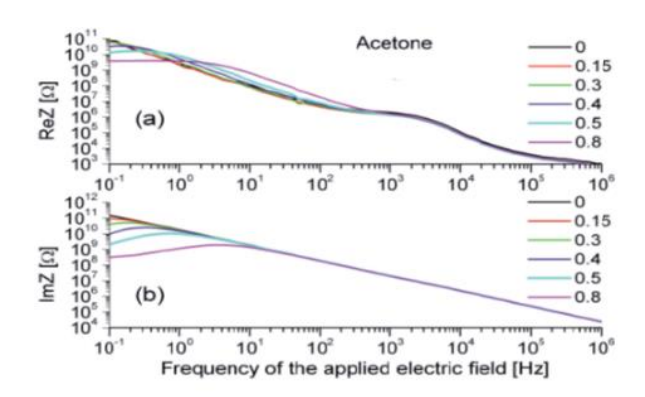


Figure 43. Representative spectra of real (a) and imaginary (b) parts of complex electrical impedance measured for DPPE LB film on SAWR-IDEs configuration upon acetone vapours at various concentrations in g/dm3 denoted on the right; 0 corresponds to vapours-free case. The temperature of the films was 25 C.

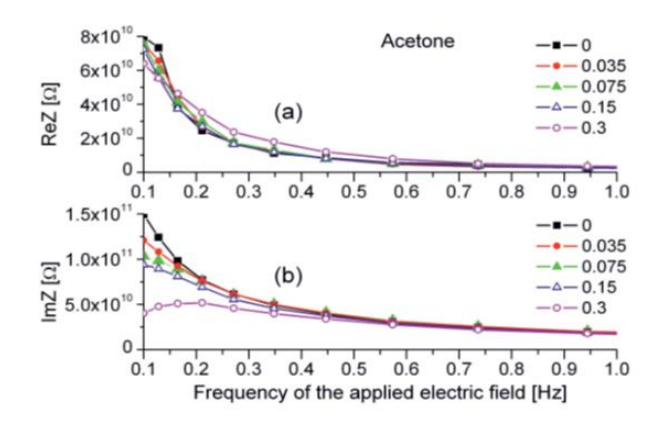


Figure 44. Representative spectra of real (a) and imaginary (b) parts of complex electrical impedance measured for DPPE LB film on SAWR-IDEs configuration upon acetone vapours at various concentrations, but at linear scale in the low-frequency region.

Figure 45 presents the frequency spectra of ReZ and ImZ measured for the studied DPPE LB film exposed to methanol vapours at various concentrations. It can be seen that in the presence of methanol vapours, the impedance values of the DPPE LB monolayer may greatly decrease. By gradually increasing concentration of methanol vapours, gradually reduced impedances are registered in the low-frequency region of the spectra. The effect is more clearly pronounced for ImZ spectra. It is well known that the decrease in ReZ(f) and ImZ(f) values toward the zero frequency is related to the decrease of the Ohmic resistance and the electrical capacitance, respectively [58 - 60]. By dielectric in capacitor-like geometry, the decrease in ReZ(f) and ImZ(f) values toward the zero frequency is caused by the electrode polarization (EP) effect. At low frequencies, this process dominates over the other dielectric polarization processes. EP is an accumulation of long-distance traveled charges at the interfaces between the electrode and the dielectric film. The observed changes of the impedance behavior were reproducible and reversible – by removal of methanol both ReZ and ImZ impedances return to the spectra corresponding to the initial vapours-free case. Because of considerable methanol gas-induced change, the impedimetric response of the examined DPPE LB films can be used for detection of methanol in gas phase.

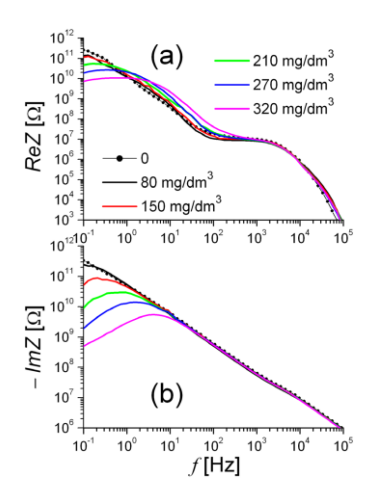


Figure 45. Frequency spectra of real ReZ (a) and imaginary ImZ (b) parts of complex electrical impedances measured for DPPE LB film deposited on interdigital electrodes, exposed to methanol vapours. The concentrations (mg/dm^3) of the vapours are shown; 0 - corresponds to methanol gas-free case. The experiment is carried out at T=26 °C

The diagrams of impedance in complex plane the Nyquist plots (-ImZ versus ReZ), obtained from the recorded impedance {ImZ(f), ReZ(f)} spectra of DPPE-NBD LB monolayers upon VOC vapours show that this EIS-presentation is also useful to indicate the impact of polar gases on such LB films deposited between/on IDEAs.

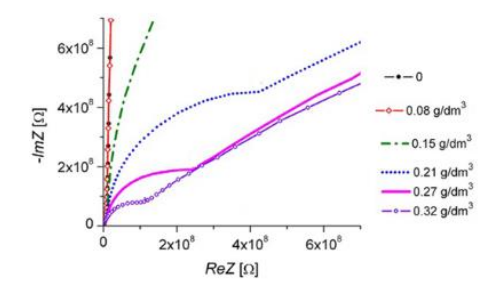


Figure 46. Nyquist plots corresponding to Z spectra in presewnce of methanol vapours.

As a representative example, Figure 46 illustrates the Nyquist plots for methanol at various concentrations of its vapours. As it is shown, the Nyquist plots consist of a depressed semicircle arc on the high-frequency side, followed by a steep line on the low-frequency side for the measured impedances. The arc-type shape corresponds to electrical conduction processes, whereas the steep line by the lowfrequency data is due to the dominant contribution of the diffusion of charged species. The latter effect is favoured by the small gap of 1.7µm between the microelectrodes used in the present work. Diffusion effect in the low-frequency region can also arise from both the layer defects and the microelectrode edges that may create in the vicinity of microelectrodes a higher-field perturbation at low frequencies. One should note that the sorption effect is dependent on the density of the LB film, as well as on its roughness and inhomogeneity (as well as those of the electrode surface). The same applies to the diffusion effect- the presence of layer defects supports the diffusion of electroactive species to the electrode surface. Further, from Figure 46 it can be seen that the semicircular portion of the Nyquist plots is shifted towards the lower resistance values. accompanied by a reduction in the size of the arc as the vapours concentration increases. Thus, the VOCs caused the capacitance of the DPPE-NBD LB monolayer to increase, and its resistance to decrease. In the Nyquist plots, the value R_{ic} of the ReZ-coordinate of the point of interception (shown with arrows in Figure 46) of the arc and at the steep line can be used as an index for the electrical conductivity (σ) of the LB film, in our case, the in-plane conductivity.

The observed decrease resistance with increasing methanol concentration is relevant for increasing the electrical conductivity of LB films.

Conclusions and Contributions

Conclusions

- ✓ Controlled modification of ionic conductance of electrolitic system PEO/PVP/NaIO₄ doped by TiO₂ nanoparticled has been achieved. Optimal change has been registered by doping of 3 wt. % TiO₂ nanoparticles. Increased ion condictiity value of electrolitic saystem PEO/PVP/NaIO₄/TiO₂ is due to improved mobility of polymer radical chains as well as to the increased quantity of dissociated polymer matrix ions.
- ✓ Doping by GO nanoparticles of mixed solid electrolite system PEO/PVP/ NaIO₄ leads to synergetic influence due to the changes at nano-surfaces' interfaces. Nanocomposite electrolite PEO/PVP/ NaIO₄/ GO posseses significantly improved ionic conductivity in relation to undoped one, which is due to surface interactions between GO nanoparticles and some functional groupes of either polymer PEO and PVP.

- ✓ Improved properties obtained by nanoparticle doping of ionic electrolites systems PEO/PVP/NaIO₄/TiO₂ and PEO/PVP/NaIO₄/GO are promissing for applications in organic electronics and electrochemical cells (Na⁺ ion polymer batteries)
- ✓ Doping of nematic LC E7 by low concentration graphene flakes (10⁻³ wt. %) leads to lower ionic conductivity as wel as dielectric permittivity due to capturing of mobile ions and reducing of the space-charge polarization. Nematic nanocomposites doped by graphene could be useful for applications in EO materials in LC daisplay technology.
- ✓ Dielectric relaxation of composites PEO/E8 и PO/E8/NaIO4 has been characterized by complex impedance and dielectric spectroscopy in frequency range 1 Hz − 1 MHz, at temperatures close to glassy state. Relaxation of dipoles has been found and compared for both types composites. Obtained results sahowed that investigated types of ion-conducting composites are perspective for applications in flexible organic electronics and energy accumulation devices.
- ✓ Doping of DPPE-NBD LB films by Cd²+ ions leads to pronounced EIS characteristics changes: lower bulk resistance (R_B) values as well as increased electric conductivity. EIS response is high enough (1 µg/L, 5 times lower than EC required health standard) to be employed as Cd²+ ions detecting method for water delivery systems as well as for quantitative ion concentration analysis.
- ✓ Obtained by us Micro-pipete technique for DPPE phospholipid monolayer preparation could be employed as electrical (EIS) detection method of chemical, biological or other substances of ecological importance.
- ✓ Volatile Organic Compound (VOC) gas molecules sorbtion on DPPE phospholipid monolayer is sensitive as well as effective enough to be detected by EIS technique employed. This sorbtion ability is due to the electrostatic interaction between the gas molecules and DPPE monolayer.
- ✓ LB type of DPPE phospholipide monolayer could be suitable molecular matrix for biological substances detection as a part of possible new micro-biosensors.

Contributions

- Micropipette-droplet technique for sensing DPPE phospholipid monolayer has been developed. The method enables needed surface contact and right localization. Obtained by us Micropipette technique for DPPE phospholipid monolayer could be employed as electrical (EIS) detection method of chemical, biological or other substances of ecological importance.
- 2. The influence of nanoparticle (TiO₂, GO) doping on polymer electrolyte system PEO/PVP/NaIO₄ characteristics have been revealed. The significant increase of its ion conductivity (near to one order of magnitude) as well as improvement of its dielectric permeability (x60) have been found.
- 3. The interaction between LB deposited film and gas molecules has been studied employing EIS technique. Bio-microsensor has been successfully elaborated. Its ability to detect convertibly VOC has been approved.
- 4. Composites of doped by nanoparticles nematics LC (E7 and E8) have been studied employing EIS and estimation of their ionic conductance and dielectric relaxation were performed. It has been found that investigated nanocomposites are perspective for application as EO materials.

List of scientific publications based on dossertation work:

 H. K. Koduru, M. T. Iliev, K. K. Kondamareddy, D. Karashanova, <u>T. Vlakhov</u>, X-Z, Zhao, N. Scaramuzza, Investigations on Poly (ethylene oxide) (PEO) – blend based solid polymer electrolytes for sodium ion batteries, Journal of Physics: Conference Series, 764, 2016, 012006 (1-8)

https://iopscience.iop.org/article/10.1088/1742-6596/764/1/012006

0.211 SJR without IF

T. E. Vlakhov, Y. G. Marinov, G. B. Hadjichristov, N. Scaramuzza
 Complex electrical impedance and dielectric spectroscopy of Na⁺-conducting PEO/PVP/NaIO₄ solid polymer electrolyte with incorporated nano-sized Graphene Oxide, Journal of Physics: Conference Series, 1762, 2021, 012010 (1-6) https://iopscience.iop.org/article/10.1088/1742-6596/1762/1/012010

0.210 SJR without IF

 Todor E. Vlakhov, Georgi B. Hadjichristov, Yordan G. Marinov, Nicola Scaramuzza Ion conductivity of nanocomposite solid polymer electrolyte PEO-PVP-NaIO₄ with added TiO₂ nanoparticles, Comptes rendus de l'Academie bulgare des Sciences, 75 (3), 2022 (349-357)

https://doi.org/10.7546/CRABS.2022.03.04

0.329 IF Q3

Todor E. Vlakhov, Yordan G. Marinov, Georgi B. Hadjichristov, Nicola Scaramuzza, Electrical conductivity properties of solid polymer electrolytes PEO-PVP-NaIO₄ filled with TiO₂ nanoparticles, Comptes rendus de l'Acad emie bulgare des Sciences, 75 (6), 2022, (804-811)

https://doi.org/10.7546/CRABS.2022.06.03

0.329 IF O3

- Todor Vlakhov, Yordan Marinov, Georgi. Hadjichristov, Alexander Petrov Electrical impedance spectroscopy of graphene-E7 liquid-crystal nanocomposite, Chemistry: Bulgarian Journal of Science Education Volume 27 Number 5, 2018 (648-657)
- G. B. Hadjichristov , <u>T. E. Vlakhov</u> , Y. G. Marinov Impedance and dielectric spectroscopy study of graphene doped liquid crystal E7, Journal of Physics: Conf. Series 1186, 2019, 012032 (1-6) https://iopscience.iop.org/article/10.1088/1742-6596/1186/1/012032

0.227 SJR without IF

 Georgi B. Hadjichristov, <u>Todor E. Vlakhov</u>, Yordan G. Marinov, Nicola Scaramuzza Ion-Conducting Flexible Thin Films of Composites from Poly(ethylene oxide) and Nematic Liquid Crystals E8—Characterization by Impedance and Dielectric Relaxation Spectroscopy, Polymers, 13 (24), 2021, 4465 (1-27)

https://doi.org/10.3390/polym13244465

4.967 IF Q1

8. <u>Todor E. Vlakhov</u>, Yordan G. Marinov, Georgi B. Hadjichristov, Nicola Scaramuzza, Electrical conductivity of composites from polymer poly(ethylene oxide) and nematic liquid crystals E8, Comptes rendus de l'Acad'emie bulgare des Sciences, 75 (8), 2022 (1115-1122)

https://doi.org/10.7546/CRABS.2022.08.03

0.329 IF Q3

G. B. Hadjichristov, Y. G. Marinov, <u>T. E. Vlakhov</u>, N. Scaramuzza
 Phospholipid Langmuir-Blodgett nano-thin monolayers: electrical response to
 Cadmium ions and harmful volatile organic compounds, Advances in
 Biomembranes and Lipid Self-Assembly, 34, Chapter 5, 2021 (129-172)
 https://doi.org/10.1016/bs.abl.2021.11.005

0.280 SJR O4

Todor E. Vlakhov, George R. Ivanov, Yordan G. Marinov, Georgi B. Hadjichristov, Phospholipid langmuir–blodgett films and impedance spectroscopy for detection of acetone and methanol vapours, Comptes rendus de l'Academie bulgare des Sciences, 74 (6), 2021 (828-834)

https://www.proceedings.bas.bg/DOI/doi2021_6_04.html

0.378 IF Q3

11. T. E. Vlakhov, G. B. Hadjichristov, Y. G. Marinov

Impedimetric response of phospholipid Langmuir-Blodgett films to methanol vapours, Bulgarian Chemical Communications, 54 (B2), 2022 (88-93)

http://www.bcc.bas.bg/bcc_volumes/Volume_54_Special_B2_2022/bcc-54-b2-88-93-vlakhov-0514.pdf

0.398 IF O4

List of scientific presentations based on dossertation work:

1. T. Vlakhov, Y. Marinov, G. Hadjichristov, G. Ivanov

Electrical impedance spectroscopy-based detection and quantification of methanol vapours by use of phospholipid Langmuir-Blodgett film (**poster presentation E.P1.**)

XXX International scientific conference "ELECTRONICS ET 2021" Sozopol, Bulgaria 15.09.2021 - 17.09.2021

2. <u>Todor E. Vlakhov</u>, Georgi B. Hadjichristov, George R. Ivanov, Yordan G. Marinov, Impedimetric response of phospholipid Langmuir-Blodgett films to methanol vapours (poster presentation P-P-7)

9-th International Scientific Conference "Modern Trends in Science" (FMNS-2021)

Благоевград, България 15.09.2021 - 19.09.2021

3. Todor E. Vlakhov, Georgi B. Hadjichristov, Yordan G. Marinov

Electrical impedance spectroscopy of sodium-ion-conducting nanocomposite solid polymer electrolytes PEO/PVP/NaIO₄/TiO₂ (oral presentation)

XXIV Winter Seminar of Young Scientists and PhD Students from the Bulgarian Academy of Sciences "Interdisciplinary Physics", Webinar Sofia, Bulgaria 07.12.2021 - 09.12.2021

4. Т. Влахов, Й. Маринов, Г. Хаджихристов

ELECTRICAL CHARACTERIZATION OF THE RESPONSE OF NANO-THIN LANGMUIRBLODGETT PHOSPHOLIPID MONOLAYER TO CADMIUM(II) IONS

(poster presentation VIII-16), XIX НАУЧНА ПОСТЕРНА СЕСИЯ ЗА МЛАДИ УЧЕНИ, ДОКТОРАНТИ И СТУДЕНТИ, XTMУ 2022, София, България, 17.06.2022

5. <u>Т. Влахов</u>, Г. Хаджихристов, Й. Маринов.

COMPLEX ELECTRICAL IMPEDANCE SPECTROSCOPY OF TiO2-NANODOPED PEO/PVP/NaIO4 POLYMER-ION ELECTROLYTE THIN FILMS

(poster presentation VIII-17) XIX НАУЧНА ПОСТЕРНА СЕСИЯ ЗА МЛАДИ УЧЕНИ, ДОКТОРАНТИ И СТУДЕНТИ, ХТМУ 2022, София, България 17.06.2022

6. Todor E. Vlakhov, Yordan G. Marinov, Georgi B. Hadjichristov.

Langmuir-blodgett phospholipid molecular monolayers: response to cadmium ions, as studied by complex electrical impedance spectroscopy (oral presentation)

XV Spring Seminar of PhD Students and Young Scientists "Interdisciplinary Chemistry" –Webinar Sofia, Bulgaria 22.06.2022 - 24.06.2022

7. <u>Todor E. Vlakhov</u>, Georgi B. Hadjichristov, Yordan G. Marinov.

Sodium-ion conducting PEO-PVP polymer blend electrolytes doped with titania nanoparticles, studied by complex electrical impedance and dielectric spectroscopy (oral presentation)

XV Spring Seminar of PhD Students and Young Scientists "Interdisciplinary Chemistry" –Webinar Sofia, Bulgaria 22.06.2022 - 24.06.202222.06.2022 - 24.06.2022

8. Todor E. Vlakhov, G. B. Hadjichristov, Y. G. Marinov.

Dielectric spectroscopy study of Na+-ion conducting PEO/E8/NaIO4 salt-complexed polymer/liquid crystals composite (**poster presentation 1-P5**)

Eleventh National Conference on Chemistry София, България 23.06.2022 - 25.06.2022

9. Yordan G. Marinov, <u>Todor E. Vlakhov</u>, Georgi B. Hadjichristov

Volatile organic compound vapor sensing with nano-thin Langmuir-Blodgett phospholipide monolayer (poster presentation 1.4.)

22nd International school on condensed matter physics "State of the art in functional materials & technologies", 29.08.2022 - 02.09.2022 Варна, България

10. Georgi B. Hadjichristov, Yordan G. Marinov, <u>Todor E. Vlakhov</u>

Thin films of nanocomposites from glassy-state tris(keto-hydrozone) discotic liquid crystals and single-walled carbon nanotubes, for optoelectronics (**poster presentation 1.11.**)

22nd International school on condensed matter physics "State of the art in functional materials & technologies", 29.08.2022 - 02.09.2022 Варна, България

11. George R. Ivanov, <u>Todor Vlakhov</u>, Evgenia Bogdanova, Georgi B. Hadjichristov, Yordan G. Marinov

Gas sensing of volatile organic compounds by Arachidic Acid Langmuir-Blodgett sensing layers and electrical impedance spectroscopy (poster presentation 1.12.)

22nd International school on condensed matter physics " State of the art in functional materials & technologies" 29.08.2022 - 02.09.2022 Варна, България

12. Todor E. Vlakhov, Georgi B. Hadjichristov, Yordan G. Marinov

Dielectric spectroscopy study of composite PEO/E8 (polymer/ liquid crystals) softmatter thin films for flexible electronics (**poster presentation 1.21.**)

22nd International school on condensed matter physics "State of the art in functional materials & technologies" 29.08.2022 - 02.09.2022 Варна, България

13. Todor Vlakhov, Yordan Marinov, Georgi Hadjichristov

NaIO4 salt-complexed PEO/PVP polymer blends with Graphene Oxide nanodopants (oral presentation № 22)

3 Национална студентска конференция по фармацевтични и химични науки 05.10.2022 - 06.10.2022 София, България

14. Т. Е. Влахов, Г. Б. Хаджихристов, Й. Г. Маринов

PEO-PVP-NAIO4-TIO2 йонно-проводящи нанокомпозитни твърди полимерни електролити (poster presentation)

IX-тата ePoster научна сесия за студенти, докторанти и млади учени 11.11.2022 София, България

15. Todor E. Vlakhov, Yordan G. Marinov

NANO-THIN PHOSPHOLIPIDIC MOLECULAR MONOLAYERS: RESPONSE TO CADMIUM IONS, AS STUDIED BY ELECTROCHEMICAL IMPEDANCE SPECTRA (oral presentation)

XIX Национална младежка научно-практическа конференция 17.11.2022 - 18.11.2022 София, България

16. Todor E. Vlakhov, Georgi B. Hadjichristov

Electrochemical impedance spectroscopy for the study of Na+-ion conducting PEO/PVP solid polymer electrolytes doped with TiO2 nanoparticles (oral presentation)

XIX Национална младежка научно-практическа конференция 17.11.2022 - 18.11.2022 София, България

17. Todor E. Vlakhov, Georgi B. Hadjichristov, Yordan G. Marinov

TiO2-nanofilled NaIO4-salt-complexed PEO/PVP polymer blend electrolytes (oral presentation)

XXVth Winter Seminar of Young Scientists and PhD Students from the Bulgarian Academy of Sciences "Interdisciplinary Physics" 06.12.2022 - 07.12.2022 Sofia, Bulgaria

18. Todor E. Vlakhov, Yordan G. Marinov, Georgi B. Hadjichristov.

Sensing of cadmium ions by Langmuir – Blodgett phospholipid molecular monolayer and complex electrical impedance spectroscopy (oral presentation)

XXVth Winter Seminar of Young Scientists and PhD Students from the Bulgarian Academy of Sciences "Interdisciplinary Physics"06.12.2022 - 07.12.2022 Sofia, Bulgaria

19. Georgi B. Hadjichristov, Yordan G. Marinov, <u>Todor E. Vlakhov</u>.

Nematic liquid crystals/polymer composites as ion conductors (**poster presentation** Nematic 12)

International NCMCT Workshop on advanced materials & technologies 28.02.2023 - 01.03.2023 Veliko Tarnovo, Bulgaria

20. Тодор Е. Влахов, Йордан Г. Маринов, Георги Б. Хаджихристов.

Твърди полимерни йонни електролити с наночастици от графенов окис (poster presentation)

51-ва Национална конференция по въпросите на обучението по физика 10.04.2023 - 13.04.2023 София, България

21. Todor E. Vlakhov, Yordan G. Marinov, Georgi B. Hadjichristov.

Mg2+-ion-conducting PEO/5CB/MgCl2 salt-complexed polymer/liquid-crystal composites (oral presentation)

XVI Spring Seminar "Interdisciplinary Chemistry" 24.04.2023 - 25.04.2023 София, България

22. Boyko Katranchev, Minko Petrov, Haritun Naradikian, <u>Todor Vlakhov</u>, Marco Castriota.

Dimeric liquid crystal nanocomposites functionalized by graphene oxide and amide graphene oxide (poster presentation)

16th European conference on liquid crystals 10.07.2023 - 14.07.2023 Rende, Italy

23. Todor Vlakhov

To what extent the EU is an effective security actor in dealing with the hybrid threats in and around Europe? (Ece)

Jean Monnet Summer School

The EU and Hybrid Threats in the Wider Neighbourhood, 4-15 September 2023 Istanbul Turkey

24. Todor E. Vlakhov, Yordan G. Marinov, Georgi B. Hadjichristov

Ion conductivity of $PEO/5CB/MgSO_4$ salt-complexed polymer/liquid crystal flexible composite electrolyte (oral presentation)

XXVI Winter Seminar "INTERDISCIPLINARY PHYSICS" for young scientists and doctoral students 09-10 декември 2023 г. Копривчица, България

Found citations related to the dissertation work: 55 items

References used in dissertation summary

- [1] Петров, А. Г., Физика на живата материя. Течнокристален подход (АИ ,,Проф. Марин Дринов'') (2014).
- [2] Collings, P. J., Goodby, J. W., Introduction to Liquid Crystals (Boca Raton, FL: CRC Press) (2019).
- [3] De Gennes, P. G., Prost, J., The Physics of Liquid Crystals (Oxford: Clarendon) (1993).
- [4] Blinov, L. M., Structure and Properties of Liquid Crystals (New York, NY: Springer) (2010).
- [5] www.sigmaaldrich.com
- [6] Bouriche, A., Alachaher-Bedjaoui, L., Barrera, A., Staelens, J-N., Maschke, U., Thermal Degradation Studies of Poly(2-ethyl hexyl acrylate) in the Presence of Nematic Liquid Crystals, Polymers, 15(19), 3934 (2023).
- [7] Jafari, A., Ghanadzadeha, A., Tajalli, H., Yeganeha, M., Moghadam, M., Electronic absorption spectra of cresyl violet acetate in anisotropic and isotropic solvents, Spectrochimica Acta Part A 66 (2007).

- [8] Koduru, H. K., Marinov, Y. G., Hadjichristov, G. B., Scaramuzza, N., Characterization of polymer/liquid crystal composite based electrolyte membranes for sodium ion batteryapplications, Solid State Ionics 335, 86–96 (2019).
- [9] https://en.wikipedia.org/wiki/Dipalmitoylphosphatidylethanolamine
- [10] da Silva, G. M. G., Faia, P. M., Mendes, S. R., Araújo, E. S., A Review of Impedance Spectroscopy Technique: Applications, Modelling, and Case Study of Relative Humidity Sensors Development, Appl. Sci., 14, 5754 (2024).
- [11] Lazanas, A. Ch., Prodromidis, M. I., Electrochemical Impedance Spectroscopy-A Tutorial, ACS Meas. Sci. Au, 3, 162–193 (2023).
- [12] Докторантски Курс : Електрохимична импедансна спектроскопиятеоретични основи и някои приложения, Лектор: проф. Дария Владикова (2022).
- [13] EC-Lab software Techniques and Applications manual, Bio Logic science instruments (2014).
- [14] Agrawal, R. C., Hashmi, S. A., Pandey, G. P., Electrochemical cell performance studies on all-solid-state battery using nano-composite polymer electrolyte membrane, Ionics 13, 295–298 (2007).
- [15] Kremer, F., Schönhals, A., Broadband Dielectric Spectroscopy Berlin: Springer (2003).
- [16] Garbovskiy, Y., Glushchenko, I., Nano-Objects and Ions in Liquid Crystals: Ion Trapping Effect and Related Phenomena, Crystals 5 501–533 (2015).
- [17] Urbanski, M., On the impact of nanoparticle doping on the electro-optic response of nematic hosts, Liq. Cryst. Today 24 102–115 (2015).
- [18] Hegmann, T., Qi, H., Marx, V. M., Nanoparticles in Liquid Crystals: Synthesis, Self-Assembly, Defect Formation and Potential Applications, Journal of Inorganic and Organometallic Polymers and Materials 17 483–508 (2007).
- [19] Lagerwall, J. P. F., Scalia, G., "Liquid Crystals with Nano and Microparticles", Nanoparticles in Liquid Crystals ,(World Scientific Publishing Co., Singapore) chapters 13–22 pp. 461–771 (2017).

- [20] Geim, A. K., Novoselov, K. S., The rise of graphene, Nature Materials 6 183–191 (2007).
- [21] Issi, J.-P., Araujo, P. T., Dresselhaus, M. S., Electron and phonon transport in gaphene in and out of the bulk (pp. 65 112). In: Aoki, H. & Dresselhaus, M.S. (Eds.). Physics of graphene. Heidelberg: Springer (2014).
- [22] De Vleeschouwer, H., Verweire, B., D'Have, K., Zhang, H., Electrical and optical measurements of the image sticking effect in nematic LCD'S, Mol. Cryst. Liq. Cryst., 331, 567 (1999).
- [23] Sasaki, N., A new measurement method for ion density in TFT-LCDs. Mol. Cryst. & Liq. Cryst. Sci. & Tech., 367, 671 679. (2001).
- [24] Baik, I.-S., Jeon, S. Y., Lee, S. H., Electrical-field effect on carbon nanotubes in a twisted nematic liquid crystal cell, Appl. Phys. Lett., 87, art. no. 263110. (2005).
- [25] Rahman, M., Lee, W., Scientific duo of carbon nanotubes and nematic liquid crystals, J. Phys. D: Appl. Phys., 42, art. no. 063001 (2009).
- [26] Garbovskiy, Y., Glushchenko, I., Nano-Objects and Ions in Liquid Crystals: Ion Trapping Effect and Related Phenomena, Crystals 5 501–533 (2015).
- [27] Said S. M., Sahamir, S. R., Sabri, M. F. M., Kamarudin M. A., Hayashi K., Polymer electrolyte liquid crystal mixtures as phase-dependent thermoelectric materials, Mol. Cryst. Liq. Cryst., 642(1), 9–17 (2017).
- [28] Kamarudin M. A., Khan A. A., Said, S. M., Qasim M. M., Wilkinson T. D., Composite liquid crystal-polymer electrolytes in dye-sensitised solar cells: effects of mesophase alkyl chain length, Liq. Cryst., 45(1), 112–121 (2018).
- [29] Kim T. H., Kim M., Manda R., Lim Y. J., Cho K. J., Flexible liquid crystal displays using liquid crystal-polymer composite film and colorless polyimide substrate, Curr. Opt. Photonics, 3(1), 66–71 (2019).
- [30] Lin J. D., Zhang Y. S., Lee J. Y., Mo T. S., Yeh H. C., Electrically tunable liquid-crystal-polymer composite laser with symmetric sandwich structure, Macromolecules 53(2), 913–921 (2020).

- [31] Pozhidaev E. P., Kaznacheev A. V., Torgova S. I., Kesaev V. V., Barbashov V. A., Polymer dispersed liquid crystals with electrically controlled light scattering in the visible and near-infrared ranges, Opt. Mater. Express, 10(12), 3030–3040 (2020).
- [32] Hadjichristov G. B., Marinov Y. G., Ivanov T. E., Koduru H. K., Scaramuzza N., "PEO/E8 Polymer-Liquid Crystal Flexible Complex Blend Electrolyte System for Na Ions", Liquid and Single Crystals: Properties, Manufacturing and Uses, (Nova Science Publ.: New York, NY, USA) ed Goosen, J., pp. 1–64 (2020).
- [33] Ailincai, D., Pamfil, D., Marin, L., Multiple bio-responsive polymer dispersed liquid crystal composites for sensing applications, J. Mol. Liq., 272, 572–582 (2018).
- [34] Jain, A. K., Deshmukh, R. R., An overview of polymer-dispersed liquid crystals composite films and their applications. In: Liquid Crystals and Display Technology (eds M. S. Ghamsari, I. Carlescu), London, IntechOpen, 11–78 (2020).
- [35] Ailincai, D., Pamfil, D., Marin, L., Multiple bio-responsive polymer dispersed liquid crystal composites for sensing applications, J. Mol. Liq., 272, 572–582 (2018).
- [36] Jain, A. K., Deshmukh, R. R., An overview of polymer-dispersed liquid crystals composite films and their applications. In: Liquid Crystals and Display Technology (eds M. S. Ghamsari, I. Carlescu), London, IntechOpen, 11–78 (2020).
- [37] ANNEX 4, "Analytical methods and achievability", Guidelines for Drinking-Water Quality: Fourth Edition Incorporating the First Addendum, (World Health Organization, WHO Press, Geneva), pp. 476–484 (2017).
- [38] "Guidelines for drinking-water quality, Fourth Edition Incorporating the first addendum", Chemical Fact Sheets Cadmium WHO Library Cataloguingin- Publication Data, (World Health Organization, WHO Press, Geneva), Chapter 12, pp. 327–328 (2017).
- [39] Klaassens, E., Kros, H., Romkens, P., Vries, W. de, Hulsmann, A., Schellekens, J., Evaluation of the EU drinking water directive, Ecorys (2015).
- [40] Waalkes, M. P., Rehm, S., Cadmium and prostate cancer, J. Toxicol. Environ. Health 43, 251–269 (1994).

- [41] Saini S., Dhania G., "Cadmium as an environmental pollutant: ecotoxicological effects, health hazards, and bioremediation approaches for its detoxification from contaminated sites", Bioremediation of Industrial Waste for Environmental Safety, Volume II: Biological Agents and Methods for Industrial Waste Management, eds.R. Bharagava, G. Saxena(Springer Nature Singapore Pte Ltd, Singapore), pp. 357–387 (2020).
- [42] "Cadmium and health: a toxicological and epidemiological appraisal", Exposure, Dose and Metabolism, Vol. 1, eds. L. T. Friberg, C. G. Elinder, T. Kjellstrom, G. F. Nordberg (CRC Press, Boca Raton, FL), (1985). and Effects and Response, Vol. 2, eds. L. T. Friberg, C. G. Elinder, T. Kjellstrom, G. F. Nordberg (CRC Press, Boca Raton, FL) (1986).
- [43] Jarup, L., Berglund, M., Elinder, C.G., Nordberg, G., Vanter, M., Health effects of cadmium exposure—a review of the literature and a risk estimate, Scand. J. Work Environ. Health, 24, 1–51 (1998).
- [44] "Cadmium in Drinking-Water", Guidelines for Drinking-Water Quality, (WHO Press, World Health Organization, Geneva, Switzerland) (2011).
- [45] Khosraviani, M., Pavlov, A. R., Flowers, G. C., Blake, D. A., Detection of heavy metals by immunoassay: optimization and validation of a rapid, portable assay for ionic Cadmium, Environ. Sci. Technol., 32, 137–142 (1998).
- [46] Pujol, L., Evrard, D., Groenen-Serrano, K., Freyssinier, M., Ruffien-Cizsak, A., Gros, P., Electrochemical sensors and devices for heavy metals assay in water: the French groups contribution, Front. Chem., 2, 1–24 (2014).
- [47] Shtenberg, G., Massad-Ivanir, N., Segal, E., Detection of trace heavy metal ions in water by nanostructured porous Si biosensors, Analyst, 140, 4507–4514 (2015).
- [48] Vikesland, P. J., Nanosensors for water quality monitoring, Nat. Nanotechnol. 13, 651–660 (2018).
- [49] Xiang, H., Cai, Q., Li, Y., Zhang, Z., Cao, L., Li, K., Yang, H., Sensors applied for the detection of pesticides and heavy metals in freshwaters, J. Sens. 2020, 8503491, 1–22 (2020).

- [50] Davey, C. L., Kell, D. B., The influence of electrode polarisation on dielectric spectra, with special reference to capacitive biomass measurements: I. Quantifying the effects on electrode polarisation of factors likely to occur during fermentations, Bioelectrochem. Bioenerg. 46 91–103 (1998).
- [51] Raicu, V., Feldman, Y., Dielectric Relaxation in Biological Systems: Physical Principles, Methods, and Applications, (Oxford University Press, Oxford) (2015).
- [52] Pichot, R., Watson, R. L., Norton, I. T., Phospholipids at the interface: current trends and challenges, Int. J. Mol. Sci. 14(6), 11767–11794 (2013).
- [53] Angione, M. D., Magliulo, M., Cotrone, S., Mallardi, A., Altamura, D., Volatile general anesthetic sensing with organic field-effect transistors integrating phospholipid membranes, Biosens. Bioelectron. 40(1), 303–307 (2013).
- [54] Wan, X. J., Mu, W., Han, X. J., Preparation methods for phospholipid vesicle arrays and their applications in biological analysis, Chinese J. Anal. Chem. 47(8), 1134–1144 (2019).
- [55] Ivanov, G. R., Georgiev, G., Lalchev, Z., Fluorescently Labeled Phospholipids New Class of Materials for Chemical Sensors for Environmental Monitoring Relevant Perspectives in Global Environmental Change", ed J I Agboola (London: InTech Int.) chapter 6 pp 89 112 (2011).
- [56] Roberts, G. G., Langmuir-Blodgett films, Plenum Press, New York (1990).
- [57] Petty, M. C., Langmuir–Blodgett Films: An Introduction, Cambridge University Press, Cambridge (1996).
- [58] MacDonald, J. R., in: Impedance Spectroscopy-Emphasizing Solid Materials and Systems, J. R. Macdonald (ed.), John Wiley and Sons Inc., New York, p. 13. (1987).
- [59] Barsoukov, E., MacDonald, J. R., Impedance Spectroscopy: Theory, Experiment, and Applications, Wiley, Hoboken (2005).
- [60] Lvovich, V. F., Impedance Spectroscopy: Applications to Electrochemical and Dielectric Phenomena, John Wiley & Sons, Inc., Hoboken (2012).